Materials Advances

ROYAL SOCIETY OF CHEMISTRY

REVIEW

View Article Online
View Journal | View Issue

Cite this: *Mater. Adv.*, 2025, **6**, 7748

Chromic Schiff bases: transformative stimuli-responsive systems for next-generation soft materials

Dimpi Gupta,†[a] Divyanshu Singh,†[b] Anushka Koranne,†[a] Chandni Singh,[a] Sunil Kumar Singh,*[a] Rajat Pratap Singh[b] and Ashish Kumar Singh *[a]

Stimuli-responsive systems, which are often hailed as "smart" materials, have garnered significant attention over recent decades due to their remarkable dynamic reactivity towards numerous external triggers. Among these, Schiff bases, due to the presence of a distinctive imine group (C=N), formed through a condensation reaction between an aldehyde or ketone and a primary amine, have become especially captivating. In addition to offering a cost-effective and easily accessible synthesis, these Schiff bases also demonstrate extraordinary chromic properties. On providing various triggers such as mechanical stress (mechanochromism), temperature variations (thermochromism), solvent change (solvatochromism), and pressure (piezochromism), Schiff bases show vivid colour changes, thus demonstrating their remarkable versatility. These chromic shifts can be attributed to reversible modifications in molecular conformation, electronic states, and intermolecular interactions within the Schiff base framework. The intrinsic ability of Schiff bases to respond and adapt to environmental changes makes them compelling candidates for the development of next-generation soft materials, with applications ranging from high-sensitivity sensors and adaptive displays to self-healing materials. Their multi–stimuli responsive behaviour opens up pathways for innovations in self-healing coatings, where damaged materials can autonomously repair themselves upon exposure to heat or pressure. This review dives deeply into the intricate mechanisms responsible for their stimuli-responsive behaviour and presents a futuristic approach to enhance their performance, highlighting them at the forefront of future stimuli-responsive and self-healing technologies.

Received 7th February 2025,
Accepted 8th August 2025

DOI: 10.1039/d5ma00109a

rsc.li/materials-advances

1. Introduction of soft materials

Our autonomic nervous system's responsive behaviour towards even a slight fluctuation in the surroundings such as temperature, pressure, light, *etc.*, is interesting for scientists in the development of analogous materials, which may mimic the natural biological system and respond to an external stimulus by changing shape, form, colour, *etc.*[1–3] Over the years, many such materials, also known as soft materials, have been developed and employed in various fields such as sensors, adaptation (ability to change behaviour in response to external stimuli), biomedical (facilitating biological functions), actuation (mimic the flexibility), and reconfiguration (transformation of patterned structure) and so on.[4–10]

These materials can be deformed and folded from 2D to 3D in the presence of an external stimulus and typically exhibit low stiffness and high flexibility compared to traditional, hard materials such as metals and ceramics. These materials include polymers, gels, colloids, foams, biological materials, and liquid crystals. These materials have intrinsic characteristics, enabling them to exhibit actuation and folding behaviour; they can be combined to generate independent and cooperative responses to external stimuli. Diverse folding structures can be realized through the rational design of geometries and the choice of materials. The reprogrammability of shape-memory polymers is appropriate to design arbitrarily reconfigurable devices. The anisotropy of liquid crystal elastomers makes it possible to create high-strength and high-speed actuators with high energy efficiency.[11–21]

Among the various materials, Schiff bases, which were first synthesized by Hugo Schiff in 1864, are of immense importance due to their easy synthesis, high yield, low-cost, high thermodynamic stability and practical applicability. The imine bond present in Schiff bases not only combines two distinct moieties, aldehyde or ketone and amine, but also has binding capabilities with metal ions and may stabilize metal ions in various oxidation states through the formation of metal complexes.

[a] *Department of Chemistry, Guru Ghasidas Vishwavidyalaya, Bilaspur 495009, Chhattisgarh, India. E-mail: ashish.bhuchem@gmail.com, aashish.bhuchem@gmail.com*
[b] *Department of Biotechnology, Guru Ghasidas Vishwavidyalaya, Bilaspur 495009, Chhattisgarh, India*
† These authors contributed equally to this work.

Possibilities of structural deformation, proton transfer, different crystalline/amorphous phases and dynamic bonds, make Schiff-bases suitable stimuli-responsive materials.[18,19] Imine bonds of Schiff bases may undergo reversible formation and cleavage under mild conditions, which is essential for dynamic covalent chemistry (DCC) allowing these materials to adapt, heal, and reconfigure in response to various external stimulus. The introduction of other functional groups and heteroatoms can easily enhance luminescent properties, making them useful for biological activity, analytical chemistry, catalysis and fluorescent material synthesis.[20,22–28]

In recent years, not only Schiff bases but also their metal complexes have been utilized for various potential applications *e.g.*, iron-chelators, anticancer agents, corrosion inhibitors, sensors, catalysts as well as stimuli-responsive materials.[14–17,22,23,29–32] The complexes based on Schiff bases exhibited as better thermodynamic stability, due to isomerization of these bases to keto form and enol form. The fluorescence of Schiff base molecules can be tuned by the inhibition of C=N isomerization by complexation with metal ions. Due to the overlap of atomic orbitals (AOs) of metal and ligands, Schiff base metal complexes usually exhibit fast proton conduction/migration and charge transfer. Several external stimuli may influence the charge transfer processes of Schiff base complexes; they have been found to respond to multiple stimuli such as temperature, pressure, light, *etc.* Due to these responses, Schiff base complexes may be appropriate for molecular switches, non-linear optics, high-density information storage, and displays.[33,34]

Schiff base-based polymers are a major leap in terms of advancing multi–stimuli-responsive materials. They respond to pH, temperature, and light, and their adjustable mechanical properties make them ideal for various applications in materials science and biomedical engineering. Since the dynamic and reversible covalent bonds of Schiff bases, easily formed under mild conditions, can have ability of self-repair after disruption in physiological environments. Self-healing polymers utilizing Schiff base bonds represent a reliable approach due to their simple and effective self-healing mechanism.[21,35] Several hydrogels have been created using these concepts which have wide potential applications in the fields of temperature control materials, anti-fatigue materials and flexible sensors, information transmission, anti-counterfeiting applications, monitoring food spoilage, biomedical applications, self-healing, anti-freezing, and conductive elastomer, *etc.*[28,36–40]

Based on the responsiveness of Schiff base-based systems (Schiff bases, Schiff-base complexes, Schiff base-based polymers) towards various external stimuli, the recent development in this field has been summarized in this review article. To the best of our knowledge, there are only a few studies on self-healing Schiff bases, as well as electrochemical, metal ion sensors, and optical diodes, but there is no review summarizing Schiff bases' role as external responsive materials. In this review, we first outline the many kinds of external stimuli and the Schiff base's mechanism of responsiveness. We then discuss several uses of known Schiff base-based systems for industrial, environmental, and biological purposes. We make an effort to cover the most pertinent references in these domains and give the scientists working in these fields the necessary background information.

2. Types of stimuli behaviour

Intelligent systems can sense their environment, process information, and respond appropriately. In nature, numerous biological systems, such as humans, animals, and cells, are viewed as intelligent.[41–46] For artificial systems, intelligence is accomplished through highly complex electronic devices, like computers and robots, which are powered by advanced algorithms.[47–49] When studying or discussing stimuli-responsive materials, the focus is primarily on those that can alter their properties in response to external stimuli without needing any additional power source or external energy input. These materials respond solely to environmental changes such as temperature, light, pH, and so on. Another approach involves using the stimulus to initiate the system's internal energy storage process. Researchers worldwide have developed a range of innovative and highly functional systems by utilizing stimuli-responsive materials as building blocks for creating more complex systems.[50] Schiff base materials are known for their impressive responsiveness to external stimuli because of their capacity for reversible reactions and sensitivity to environmental changes, which makes them essential for developing smart materials used in fields like tissue engineering,[51] drug delivery,[51] fire safety, thermal energy management,[52] shape memory function,[53] responsive liquid material,[33] 2D to 3D encryption[37] *etc.* In this review, we have discussed four major external stimuli: mechanical, temperature, stress–strain, and solvent, because these four responsive behaviours are pillars for generating smart materials. In addition to these, multiple stimulus responses for some Schiff base compounds are also discussed.

2.1 Mechanochromism

As the name suggests, mechanochromism refers to a change in a material's colour upon exposure to external mechanical stimulus. The luminescence can arise from external forces such as crushing, rubbing, or even grinding which eventually lead to a reversible change in colour or fluorescence, and thus making them a suitable candidate in a diverse range of applications such as in sensors, bio-imaging, anti-counterfeiting, fluorescent encryption writing, *etc.*[53–58] Modification of emission properties arises due to either an increase in the intermolecular interaction or due to the breakage of certain interactions due to applied mechanical force. These mechanical forces, such as smashing, shearing, or grinding, affect the emission wavelength or the fluorescence quantum yield, leading to the observation of high-contrast luminescence colour.[59,60]

The applied force sometimes causes conformational changes, as well as the conversion of compounds from a crystalline to an amorphous state,[55,61,62] or even from one crystalline state to another. This leads to changes in certain interactions, such as hydrogen bonding and charge transfer processes, ultimately affecting the emission.[63,64] Various

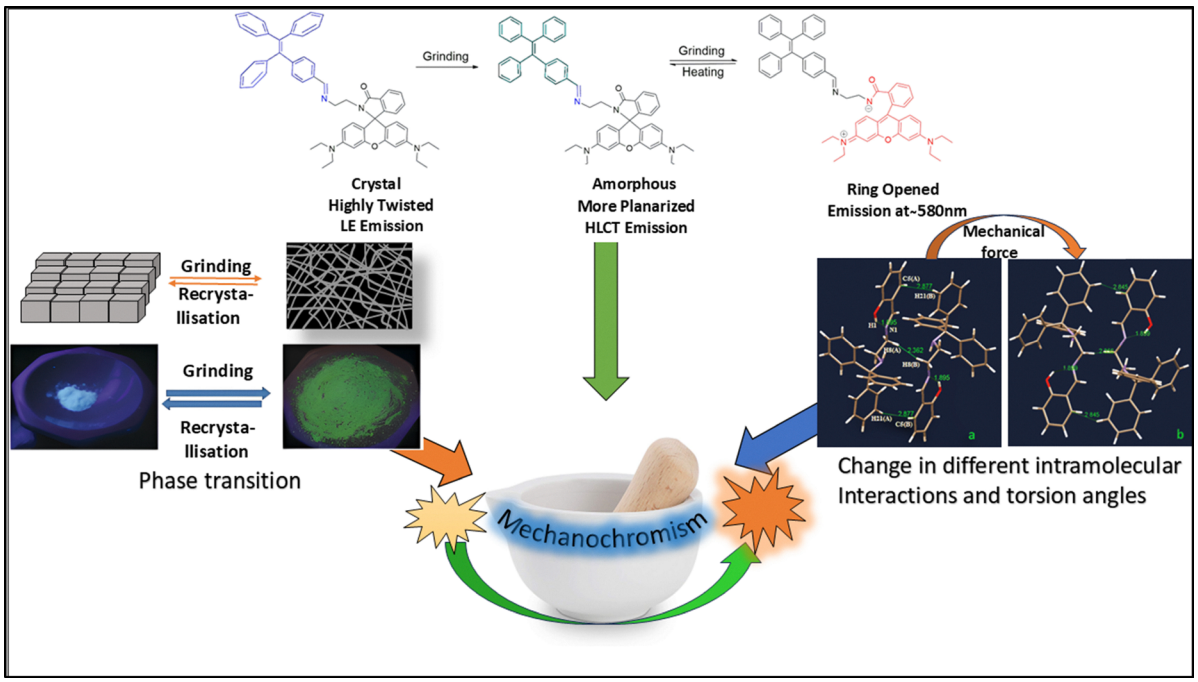

Fig. 1 Mechanochromic behaviour *via* phase transition, conformational changes; redrawn from ref. 65 with permission from ACS, Copyright 2016, and different torsion angles; reproduced from ref. 66 with permission from RSC, copyright 2017.

mechanisms related to mechanochromism—such as phase transitions, changes in molecular interactions through torsion angle variations, and conformational changes that alter fluorescence responses—are illustrated in Fig. 1.

Additionally, many mechanochromic Schiff base systems involving triphenylamine, TPE moiety, salicylaldehyde, hydrazone, azide, nicotine hydrazide, naphthalene, *etc.*, which have applications in smart devices and sensing, are shown in Scheme 1. Their applications are further discussed in Section 5 of this review in the form of a table. These changes in phase upon grinding can be confirmed using the powder X-ray diffraction (PXRD) analysis. The sharp and intense peaks of the pristine sample often diminish into weak and broad diffraction peaks or even disappear upon grinding, showing the destruction of a systematic arrangement with breakage of weak interactions, accompanied by a red-shift emission.[57] However, exposing these ground samples to heat or solvent fumigation restores the sharp peaks, demonstrating the recovery of an ordered structure from an amorphous one. These cyclic colour changes can be easily understood by their PXRD patterns. Similarly, the changes in morphology from a perfectly ordered arrangement to a partially amorphous form and back into the desired crystalline form with some minute differences can be well observed by FESEM.[56] Thus, a more flexible structure capable of undergoing smooth phase transitions becomes an ideal candidate for exhibiting excellent reversible mechanochromism. The presence of multiple rotatable aromatic rings, various intermolecular and intramolecular interactions such as π···π stacking, weak coordination bonding, and hydrogen bonding, also plays a crucial role in enhancing the mechanochromic behaviour of the Schiff base complexes. The flexibility of these aromatic rings can be further increased by introducing certain groups, such as methylene, which promote the formation of a more twisted conformation, ultimately leading to improved mechanochromism.[67] When mechanical force is applied, the bond distance between adjacent molecules as well as the dihedral angles between the aromatic rings change.[68–70] Although the presence of rotatable aromatic rings renders it a loosely packed structure by raising the dihedral angle, its excessive abundance may also induce steric hindrance, minimizing the importance of the MCL phenomenon.[67,70] In addition, a more twisted molecular conformation is facilitated by exploiting numerous inter- and intramolecular interactions, which ultimately results in high-contrast mechanochromism without undergoing a phase transition.[57] The adaptations in molecular conformations and packing modes are also accountable for the mechanism of mechanochromism at the molecular level.[71,72] The DFT studies of $\mathbf{H_4L^2}$ Schiff base also indicated the significant effect of molecular conformation on their excited state properties. Two molecular conformations are possible in the $\mathbf{H_4L^2}$ system, named $\mathbf{H_4L^2}$-y and $\mathbf{H_4L^2}$-r, and they have the same structural composition. With an intersecting type of conformation, $\mathbf{H_4L^2}$-y has its highest occupied molecular orbital (HOMO) and lowest occupied molecular orbital (LUMO) covering the molecular framework almost completely. On the other hand, $\mathbf{H_4L^2}$-r, with its almost co-planar conformation and strong intermolecular interactions, has localized HOMO and LUMO levels on the phenyl and naphthyl parts, respectively. The TD-DFT calculations showing the main absorption corresponding to the S_1–S_0 transition also indicate that the HOMO → LUMO contribution in $\mathbf{H_4L^2}$-y is lower (60.0%) than that of $\mathbf{H_4L^2}$-r (91.1%). The decrease in oscillator strength (f) during this transition from

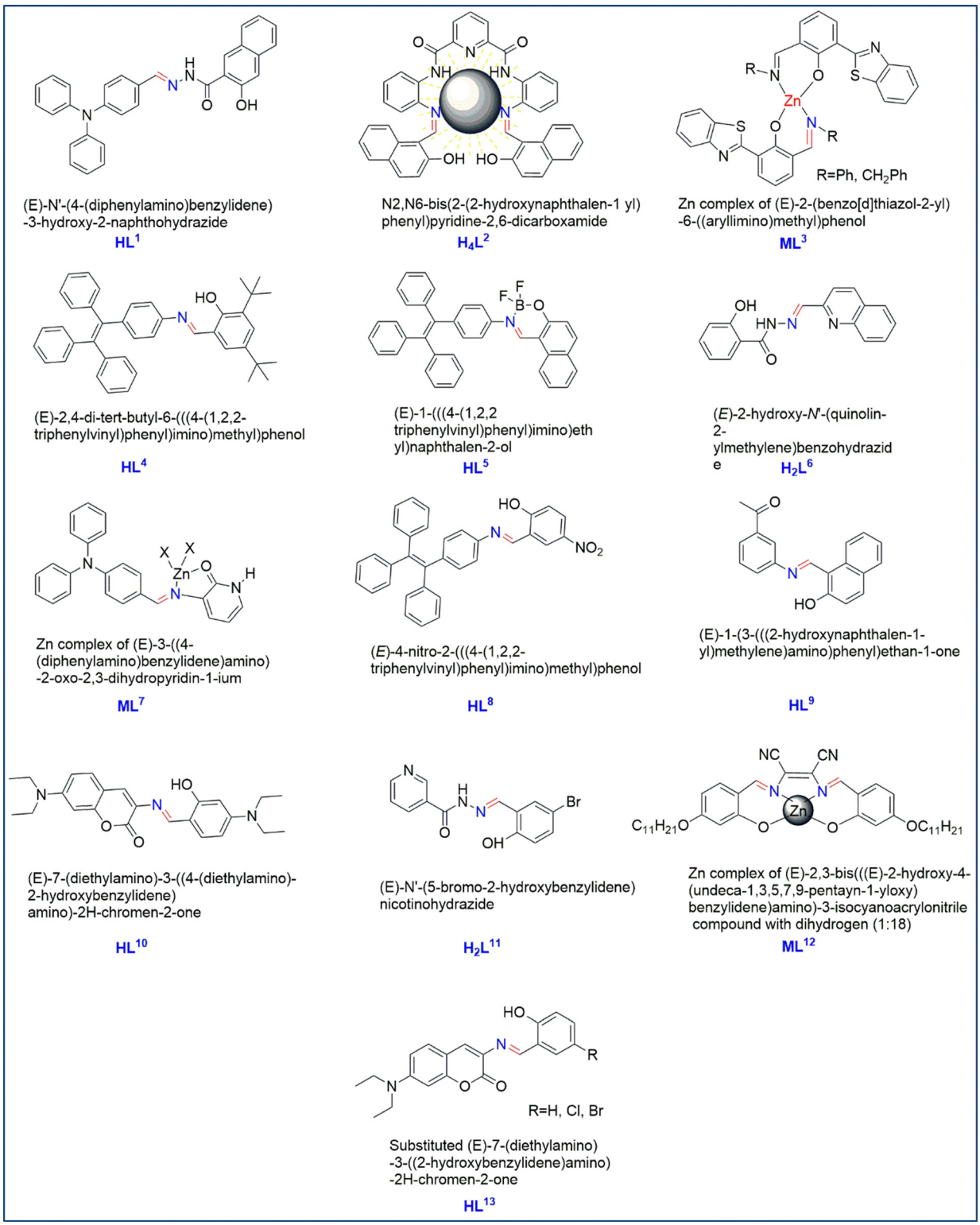

Scheme 1 Schiff base-based systems exhibiting mechano- and/or piezo-chromism.

0.1499 to 0.1273 correlates with a decrease in the twist of the dihedral angle in $\mathbf{H_4L^2}$, resulting in a decrease in emission and a red shift (Fig. 2).[57]

As shown in Fig. 3(a) and (c), the original sample of Zn complex of Schiff base $\mathbf{ML^3}$ prepared from 3-(2-benzothiazolyl)-2-hydroxybenzaldehyde showed cyan-blue emission under UV light at 480 nm. Upon slight grinding, the wavelength is shifted to 472 nm, which appears blue. If the sample undergoes significant grinding, again, a shift of wavelength could be visible to 520 nm and exhibit green colour in UV light.

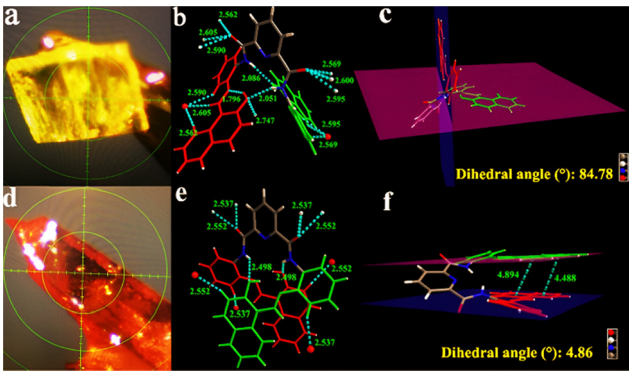

Fig. 2 Crystal photographs (a) and (d), hydrogen bonding (b) and (e), and dihedral angle (c) and (f) of H_4L^2-y and H_4L^2-r Crystal, respectively; reproduced from ref. 57 with permission from RSC, Copyright 2022.

Interestingly, if it is fumed in DCM, the sample returned to cyan emission at 472 nm. XRD spectra confirm the changes in this complex's crystalline structure (Fig. 3(b)).[70] Interestingly, **HL**^{4} shows reversible mechanofluorochromism (MFC) (mechanofluorochromism is a subtype of mechanochromism which can show changing behaviour under mechanical force stimulus; both the sample colour and the emission colour of the mechanofluorochromic materials are changed). Its emission colour changes from yellowish green to orange-yellow after grinding (Fig. 3(d)).[56] The presence of non-planar geometries and (donor) D–(acceptor) A conjugated systems gives these materials mechanofluorochromic (MFC) behaviour with excellent reversibility up to six cycles without any delay.[73] The reversible mechanochromism of Schiff base H_4L^2 based on naphthaldehyde is attributed to its flexible behaviour. Upon mechanical stimuli, *i.e.,* grinding, the bright orange emission at 540 nm undergoes a red shift to 662 nm with reduction in fluorescent time, which can be reversibly changed back to yellow by providing a CH_2Cl_2 atmosphere (Fig. 3(e)). XRD and SEM analysis confirm the changes in crystalline structure (Fig. 3(f)–(h)).[57] Similarly, force-induced reversible high-contrast colour switching from bright green emission under 365 nm to orange was also observed for the tetraphenylethene-based Schiff base ligand and its corresponding boronated complex **HL**^{5} can revert to its original emission colour by fuming with DCM (Fig. 3(i)–(k)). Another mechanochromic Zn(II) complex based on quinoline-appended acylhydrazone ligand (H_2L^6) was synthesized, whose loosely ordered stacking pattern and twisted structure allow for molecular motion change upon grinding, resulting in mechanochromism and hence the complex can be developed as an excellent material in the area of stress detection.[74]

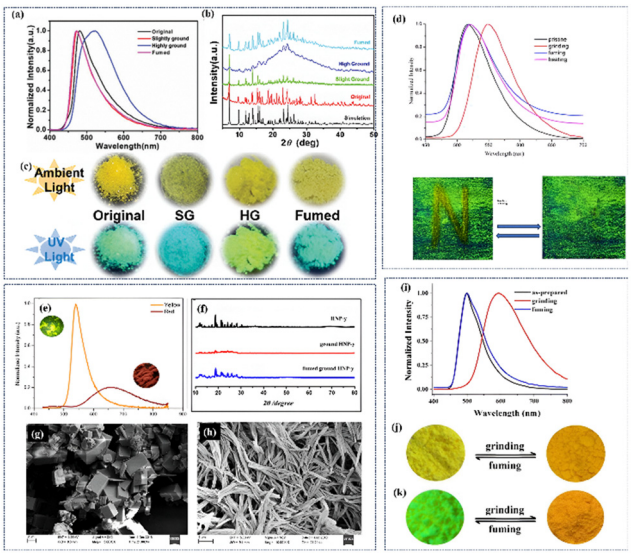

Fig. 3 Mechanoluminescence properties of Zn(II) complexes based on Schiff base **ML**^{3} (a) and (c) Fluorescence emission spectra and appearance of the sample under ambient and UV light, (b) PXRD pattern; reproduced from ref. 70 with permission from RSC, Copyright 2021; (d) fluorescence spectra at 420 nm in different solid states upon grinding and fuming/heating of **HL**^{4}; reproduced from ref. 56 with permission from Elsevier, Copyright 2019; (e) orange and red line fluorescence spectra of the naphthaldehyde Schiff base of powdered H_4L^2-y and H_4L^2-r, respectively, (f) PXRD patterns of H_4L^2-y and H_4L^2-r crystals when ground and fumed with DCM, (g) and (h) SEM image of H_4L^2; reproduced from ref. 57 with permission from RSC, Copyright 2022; (i) of **HL**^{5} showing normalized fluorescent spectra in different solid-states, ground and fumed at 365 nm (j) and (k) solid colour appearance of **HL**^{5} under ground and fumed conditions; reproduced from ref. 73 with permission from Elsevier, Copyright 2019.

2.2 Piezochromic/stress stimuli responsive material

Piezochromism is the property of a material that changes colour or becomes luminescent when subjected to mechanical stress, such as when it is compressed or ground. The material can revert to its initial state if the pressure is released.[75–77] Scheme 2 shows how the Schiff base system's systematic structure may be upset by exerting pressure, which can be released for a specific system using a specific solvent. Han *et al.* developed a tetraphenylethene-based Schiff base, (*E*)-4-nitro-2-(((4-(1,2,2-triphenylvinyl)phenyl)-imino)methyl)phenol (**HL**^{8}) using 4-tetraphenylethenylamine and 5-nitrosalicylaldehyde. The optical properties demonstrate an on–off–on switching behaviour with a distinctive U-shaped pattern when water is added to a THF solution, showcasing both TICT and AIE features. These attributes impart reversible piezofluorochromic properties to **HL**^{8}. DFT quantum chemical calculations reveal a fascinating distribution of orbitals in **HL**^{8}. The HOMO is primarily localized on the TPE unit and the central C═N bond,

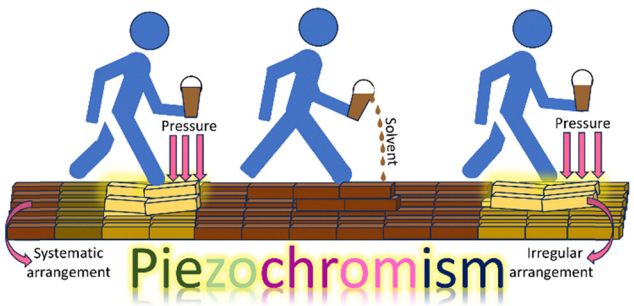

Scheme 2 Piezochromic behaviour showing reversibility of systematic arrangement to irregular arrangement on applying pressure.

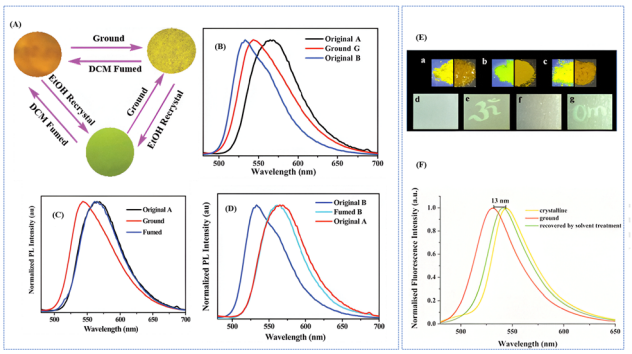

Fig. 4 (A) Schiff base **HL**[8] showing reversible piezofluorochromism in the ground (g) and crystalline states (a) and (b) using EtOH and DCM. (B) showing fluorescence spectra of original HL[8] (a) and (b) along with their powdered state (g). (C) and (D) showing photoluminescence spectra of (a) and (b) respectively after grinding and fuming process; reproduced from ref. 78 with permission from RSC Adv, Copyright 2016; (E) **HL**[9] Schiff base showing (a) crystalline, (b) ground, and (c) recovered structure by solvent, respectively, (d) dried filter paper dipped with **HL**[9] solution in ethanol. (e) ''Om'' A Sanskrit symbol written on the paper, (f) visibility of erased paper by using ethanol and then dried, (g) ''Om'' English letters written on the same paper, (F) PL spectra for crystalline, ground and recovered states by using solvent treatment; reproduced from ref. 25 with permission from Elsevier, Copyright 2018.

while the LUMO is strikingly concentrated around the 4-nitrophenol group and an adjacent phenyl ring of the TPE. This distribution highlights the distinct electronic properties across different regions of the molecule. This indicates a strong inclination for **HL**[8] to adopt a TICT state. According to the Franck–Condon principle, when the system is locally excited, the molecule's planar conformation is stabilized by electronic conjugation, particularly in nonpolar solvents. In a polar solvent, **HL**[8] undergoes a remarkable transformation from a LE state to a TICT state. This transition is facilitated by intramolecular rotation, culminating in complete charge separation between the donor and acceptor moieties. Such behaviour underscores the dynamic nature of **HL**[8]'s electronic structure in response to solvent polarity. In the aggregated state, TICT is suppressed due to restricted intramolecular rotation as the molecule adopts a planar geometry.[78] Photoluminescence studies using DCM and EtOH revealed that the two recrystallized samples exhibit reversible piezofluorochromic properties through repeated grinding and fuming processes (Fig. 4(A)–(D)).[78] We have synthesized Schiff base **HL**[9] in one of our research articles, which is based on naphthaldehyde and shows significant piezochromism in its solid state. Amazingly, when crystalline **HL**[9] is ground, its blue emission switches from 544 nm to 531 nm, and its dark yellow luminescence changes to a light green due to AIE properties. Furthermore, even after grinding, **HL**[9] maintains its good crystalline integrity. **HL**[9] is a promising candidate for pressure-jet printing and pressure sensing due to its simple synthesis and reversible transformation behaviour. A practical application was demonstrated by dipping filter paper in a Schiff base solution, where the Sanskrit symbol 'Om' was written and later erased using ethanol. The same paper could then be reused to write the English letter 'Om'. This encryption writing is a good way to express how materials could revert to their original form (Fig. 4(E) and (F)).[25]

2.3 Thermochromism

Thermochromism refers to the phenomenon where compounds exhibit a visible colour change in response to variations in temperature. Scheme 3 shows a Schiff base system that exhibits thermochromic behaviour. Temperature variation induces structural changes in molecules, interconversion of stereoisomeric forms, differences in the energy levels of LCAO, and phase transition. Alterations in molecular structure result in changes to the energy gap between the HOMO and the LUMO, which is responsible for the thermochromic properties of various organic compounds. Schiff bases and their complexes exhibit enol–imine and keto–amine tautomerism, and their structure allows for easy substitution of rings with different functional groups.[81] The ease of reversible switching from the *cis* to *trans* form upon heating also makes them suitable for exhibiting thermochromic behaviour.[81,82] Maintenance of thermal equilibrium between the original molecule and its structurally modified form of phase-change materials (PCM) makes them promising candidates for a variety of applications, including air conditioning systems, thermosensitive imaging, drug delivery systems, and wearable temperature sensors.[83–86] Conversion of molecular arrangement from one physical state to another on providing temperature stimuli makes these PCMs an efficient option for energy storage and release materials.[83] Fig. 5 shows that Schiff base-based materials can exhibit thermochromic behaviour due to the significant presence of phase transition, isomerisation, AIE property, or ESIPT mechanisms.[34,79,80,87,88] During the phase transition, the inner networks of the combined materials remain chemically cross-linked as shown in PEG-based polyurethane.[89–92] However, this permanent cross-linking in the system makes them non-recyclable and hampers the balance in shape stability and high energy storage density. By incorporating an aromatic Schiff base structure into non-recyclable parts of linear **P2** (*N*,*N*′-bis(*p*-hydroxybenzylidene-amino)phenylenediamine PEG–PU polymer), not only can PEG chains be immobilized, but they can also undergo crosslinking reactions at high temperature, thus making this PCM fire safe and endowing self-shape stabilization (Fig. 6). These PCMs, due to their reprocessability and solid–solid phase change properties, find application in self-supporting stable thermal management and anti-counterfeiting thermosensitive imaging.[52]

Du *et al.* investigated how incorporating a metal–organic framework (MOF) into a Schiff base connected to a polymeric system can enhance the proton conduction switching ratio. For their study, they selected the Schiff base 4-((2-hydroxybenzylidene)amino)-benzenesulfonic acid (**H_2L**[23]), polyvinyl alcohol (PVA), poly(2-acrylamide 2-methyl-1-propane sulfonic acid) (PAMPS), and a Zr MOF-808 composite system.[34] This integrated structure provides a well-known proton conduction pathway through the vehicle (a surplus proton may traverse the solvent on top of a host molecule in a linear way) and Grotthus mechanism (a local molecular arrangement is achieved by rotational motion after proton jumps between water molecules)

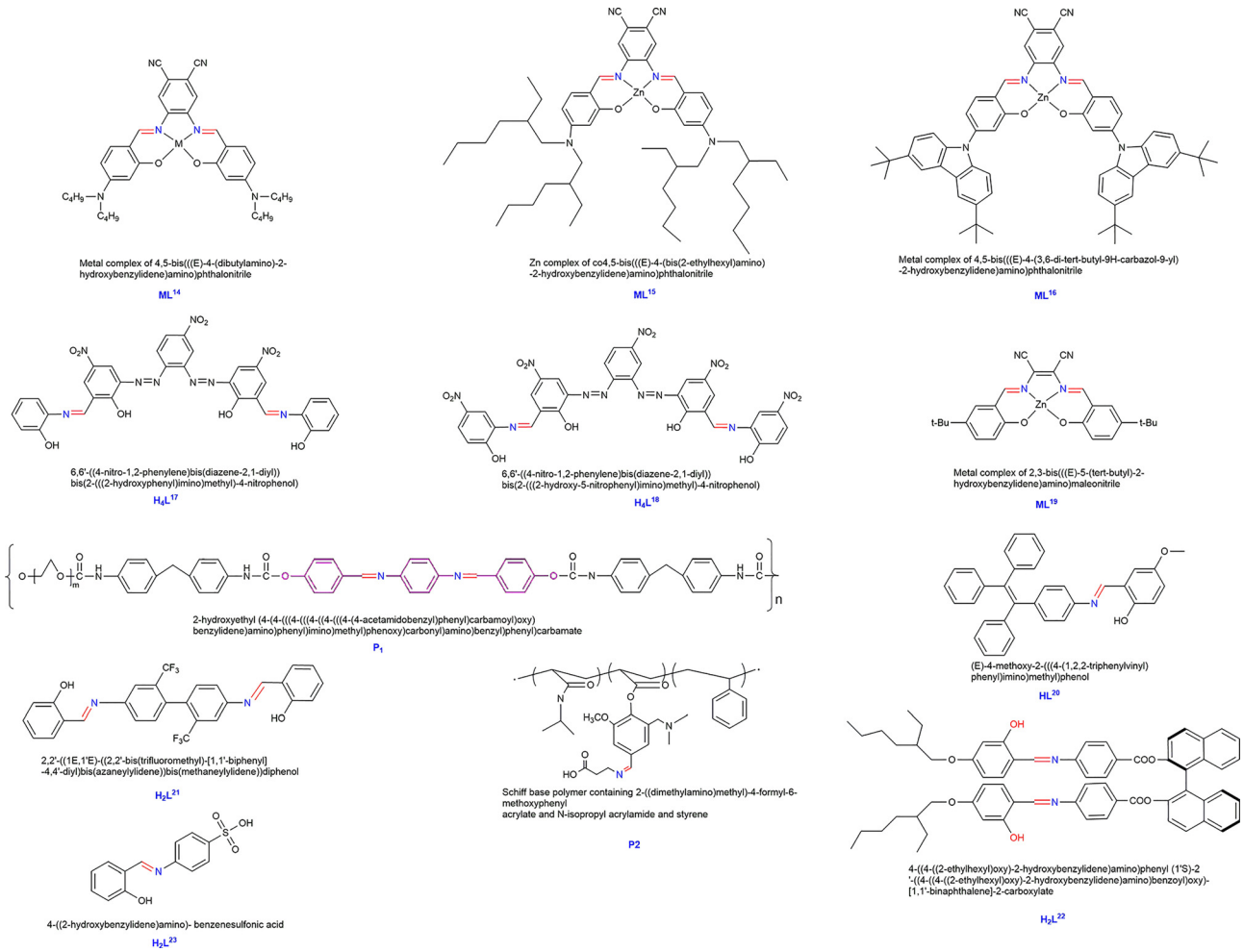

Scheme 3 Schiff base-based systems exhibiting thermochromism.

(Fig. 7).[93–95] Fluorescence measurements were employed to study isomerization linked to proton conduction. A blue shift ($\Delta\lambda$ = 10 nm) was observed as the temperature was increased, particularly in the presence of a high concentration of electron-donating groups, with $\mathbf{H_2L^{23}}$ exhibiting an emission peak at λ = 510 nm (Fig. 8(a)). Upon combining $\mathbf{H_2L^{23}}$ with MOF-808, a reversible blue shift ($\Delta\lambda$ = 20 nm) was detected in the emission spectra during heating, indicating thermally driven isomerization (Fig. 8(b)). The dissociation of H^+ ions from the sulfonic and hydroxyl groups of the polymers is thought to enhance the emission peak intensity at 353 K. Fig. 8(c)–(e) highlight notable IR spectral changes during heating at 353 K and after 5 minutes of cooling, further supporting isomerization. Additionally, UV spectroscopy was used to analyze keto/enol tautomerism in $\mathbf{H_2L^{23}}$ (Fig. 8(f)) and $\mathbf{H_2L^{23}}$@MOF-808 suspensions under thermal stimuli (Fig. 8(g)). The study revealed that MOF-808 pores favour the keto state at lower temperatures, representing the involvement of an intramolecular charge transfer (ICT) transition in this system.[34] The thermochromic and photochromic characteristics of salicylaldehyde Schiff bases ($\mathbf{H_2L^{21}}$) in the solid state have attracted a lot of attention, with a twisted structure due to thermochromic and AIE properties. Changes in colour from bright yellow to orange occur as the temperature rises, showcasing excellent reversibility even after multiple heating–cooling cycles (Fig. 9(a)–(c)). Because of keto–enol forms present in equilibrium, a colour shift is triggered by temperature changes. DSC study reveals that $\mathbf{H_2L^{21}}$ has remarkable thermochromic sensitivity, rapid response, and strong thermal stability, with clear endothermic peaks indicating phase transitions and decomposition points at 230 °C and 400 °C, respectively (Fig. 9(d)). Notably, $\mathbf{H_2L^{21}}$'s thermochromic process is gradual and heat-absorbing. Although $\mathbf{H_2L^{21}}$ lacks photochromic characteristics, probably caused by the reduced dihedral angle between aromatic rings, which limits *cis–trans* isomerization, it excels in fatigue resistance, response time, and consistency in temperature-induced colour changes.[80] Additionally, Schiff base complexes exhibiting thermochromism based on polymers, methoxy phenol, and chiral binaphthol derivative linked salicylaldehyde, have also been developed and studied for their various applications in fire safety, sensing and remote control devices, which have been discussed in Section 5 of this review.

2.4 Stress–strain responsiveness/self-healing behaviour

Advanced materials, such as stress- and strain-responsive hydrogels, exhibit significant changes in their mechanical

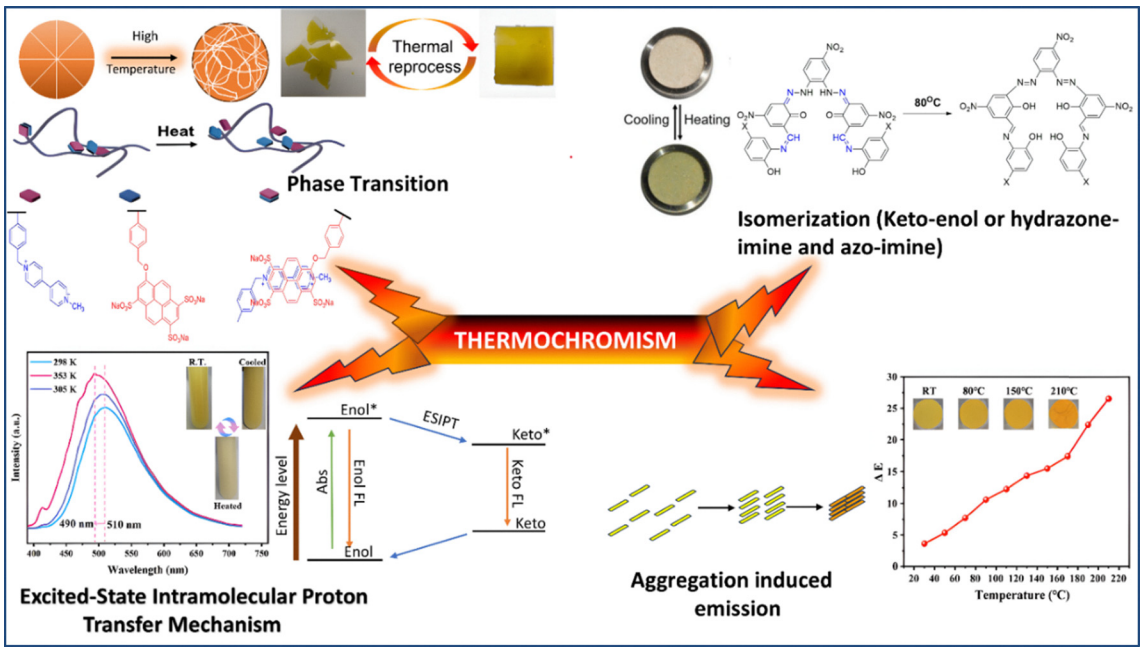

Fig. 5 Thermochromism behaviour with various mechanism phase transitions involved; reproduced from ref. 52 with permission from Elsevier; Copyright 2022, redrawn from ref. 87 with permission from Wiley, Copyright 2023; isomerization; redrawn from ref. 79 with permission from Elsevier, Copyright 2019; excited state intramolecular proton transfer mechanism (ESIPT); reproduced from ref. 34 with permission from ACS, Copyright 2023, and aggregation induced mechanism (AIE); reproduced from ref. 80 with permission from Elsevier, Copyright 2024.

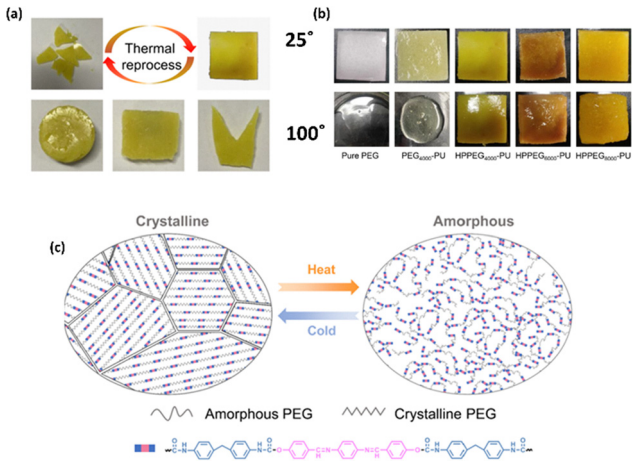

Fig. 6 Thermal reprocessing of the **P1** at 80 °C under 5 MPa for 5 min; (e) the shape stability at the melting temperature of pure PEG; (c) schematic representation of the reversible phase change property of P1; reproduced from ref. 52 with permission from Elsevier; Copyright 2022.

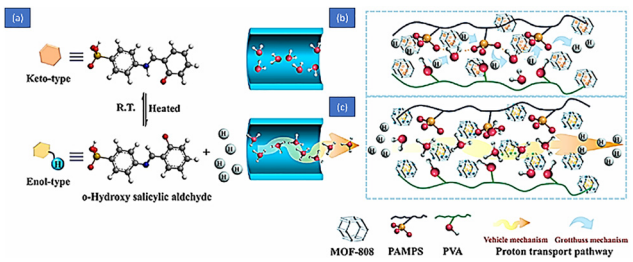

Fig. 7 Thermal-response proton transfer pathway of (a) H_2L^{23}@MOF-808 composite and their hybrid membrane (b) and (c) using the keto and enol type structure of *o*-hydroxy salicylaldehyde; reproduced from ref. 34 with permission from ACS, Copyright 2023.

and electrical properties when subjected to external pressures. Scheme 4 illustrates the Schiff base system responsible for self-healing capabilities upon the application of strain or stress. These hydrogels are ideal for use in flexible electronics, wearable sensors, and soft robotics due to their ability to detect and react to mechanical deformations. Hydrogel's ability to adapt to stress and strain is made possible *via* piezoresistive effects, in which variations in resistance are correlated with applied strain.[96] The development of hydrogels with self-healing capacity could prove beneficial since these self-healing hydrogels can recover their chemical and physical characteristics and regain their original shape, functionality, and structure after an impact.[97] The recovery is possible due to dynamic covalent bonds since it doesn't require secondary stimuli for recovery of the material to its original state.[98] Imine bonds, the most often utilized dynamic covalent link, require mild reaction conditions and a rapid reaction rate, making them suitable for tissue engineering. They are stronger than acylhydrazone and disulfide bonds and also provide impressive self-healing capacity.[99–101]

The Schiff base reaction generated the PVA–CHO–NH_2 polymer (**P7**), which contains both aldehyde and amino groups. This polymer exhibits intrinsic self-healing ability. Fig. 10(a) illustrates the self-healing mechanism of the polymer based on

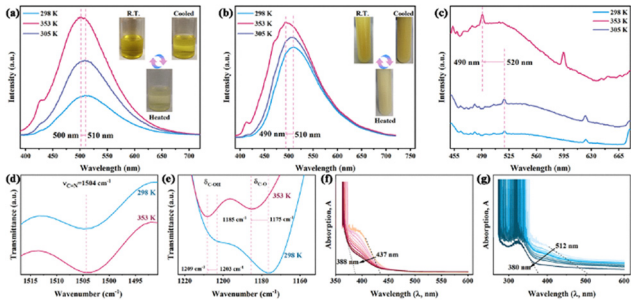

Fig. 8 Fluorescence spectra at 360 nm for the (a) H_2L^{23} solution, (b) H_2L^{23}@MOF-808 suspension, and (c) H_2L^{23}@MOF-808/PP-25 at 298 K, 353 K, and cooling for 5 min to 305 K, respectively. (d) and (e) Partial infrared spectra of H_2L^{23}@MOF-808 at room temperature and after heating at 353 K for 5 min. UV-vis absorption spectra of the (f) H_2L^{23} solution and (g) H_2L^{23}@MOF-808; reproduced from ref. 34 with permission from ACS, Copyright 2023.

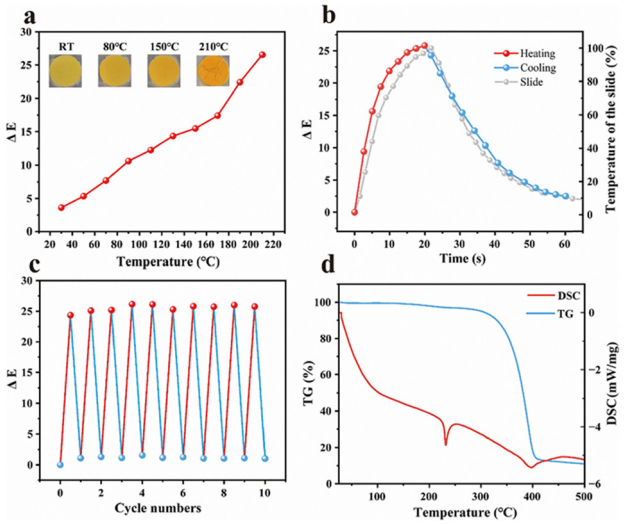

Fig. 9 H_2L^{21} showing thermochromic responsiveness (a) ΔE–T plot, (b) response time curve and temperature of the slide, (c) heating–cooling cycles, and (d) TG–DSC curve; reproduced from ref. 80 with permission from Elsevier, Copyright 2024.

dynamic Schiff base linkages. The healing time for this polymer is 24 hours.[102]

Li *et al.* synthesized a hydrogel by reacting hyaluronic acid with cystamine **P5**. They found that the strength of the hydrogel improved with the addition of cystamine, as shown in Fig. 10(b). This hydrogel was cut into three pieces and then autonomously rejoined into a single entity without any external pressure or intervention. A micro-level illustration of a hydrogel is shown in Fig. 10(c), where slits are firmly linked and eventually vanish after 40 minutes. The loaded integrated hydrogel in a syringe could be progressively injected into Teflon molds using needles with 0.5 mm diameters, as illustrated in Fig. 10(d). Thus, based on the stress after mechanical disruption, this dynamic imine bond provides the hydrogel with remarkable self-healing ability.[103] Additionally, other Schiff base complexes based on polymers such as chitosan, propionamidobenzohydrazoic acid, benzylideneaniline, and spiro moieties have also been developed for their stress–strain responsiveness and self-healing properties, which are discussed in Section 5 of this review.

Qu and co-workers have extensively researched stimuli-responsive hydrogels, developing various Schiff base hydrogels with applications in sensing, biomedical uses, and smart materials. They initially developed a quinoline-based Schiff base sensor (L^{24}) for multiple molecules and bioimaging.[104] Their work expanded into MSH with pH-responsive properties, self-healing abilities, and potential for controlled release. They investigated the distinctive properties of hydrogels, which are three-dimensional molecular networks infused with water. Hydrogel was initially introduced in 1950 for biological applications; these materials have since gained widespread interest. Hydrogels are eco-friendly and biocompatible, as their structure and composition closely mimic the extracellular matrix.[105–107] Salicylaldehyde-based Schiff bases with a polymeric system generated a hydrogel (HL^{25}), which has self-healing properties as well as outstanding stretchability and thermoresponsive behaviour. Tunable fluorescence occurs as a result of the conjugate system and may be modulated using Zn^{2+}/EDTA. Using a 0.1 M concentration of Zn^{2+}, the intensity of fluorescence increases by 640%.[28] They explored MSHs composed of an amphiphilic polymer and 2-(benzylidene-hydrazonomethyl)-phenol (**P9**), in which the Schiff base structure of **P9** exhibited pH sensitivity. One of the hydrogels they developed was specifically designed to selectively bind with Fe^{2+} and Cu^{2+} ions, exhibiting self-healing properties, which made it well-suited for biomedical applications and controlled release systems.[21,39] Further work by Qu's team led to the creation of advanced hydrogels by enhancing gelation through stronger hydrophobic interactions. Using salicylaldehyde benzoyl hydrazone (**P10**) as a hydrophobic ligand, paired with polyethylene glycol as the hydrophilic chain, they incorporated Ni^{2+} ions into the system. This hydrogel, named Ni-P10, exhibited colour changes when exposed to biogenic amine vapors, making it a highly promising candidate for food monitoring applications.[38] Their research progressed with the development of a micellar copolymer composed of acrylic acid, acrylamide, and a hydrophobic arylhydrazone-based ligand, **P11**. This resulted in a hydrogel stretching up to 5000% of its original length without breaking. By incorporating aluminum, they enhanced the hydrogel with shape-memory properties. This exceptionally stretchable and multifunctional hydrogel has great potential for use in information transmission, wearable devices, and flexible sensors.[108] Another notable breakthrough was the development of a cross-linked gelatin/metal complex integrated with a poly(acrylamide-acrylate) double network gel **P12**. This system exhibited Fe^{3+} and H^+-responsive fluorescence quenching, temperature- or Fe^{3+}-induced shape memory, and self-healing capabilities. Utilizing these features, the researchers created various multistage data encryption platforms, extending from 2D to 3D encryption, showcasing the potential of smart fluorescent hydrogels in high-security anti-counterfeiting applications.[37] Pyridine-hydrazone and pyridine-dicarbohydrazone-based cross-linkers, derived from Schiff bases, display multi–stimuli-responsive properties and offer

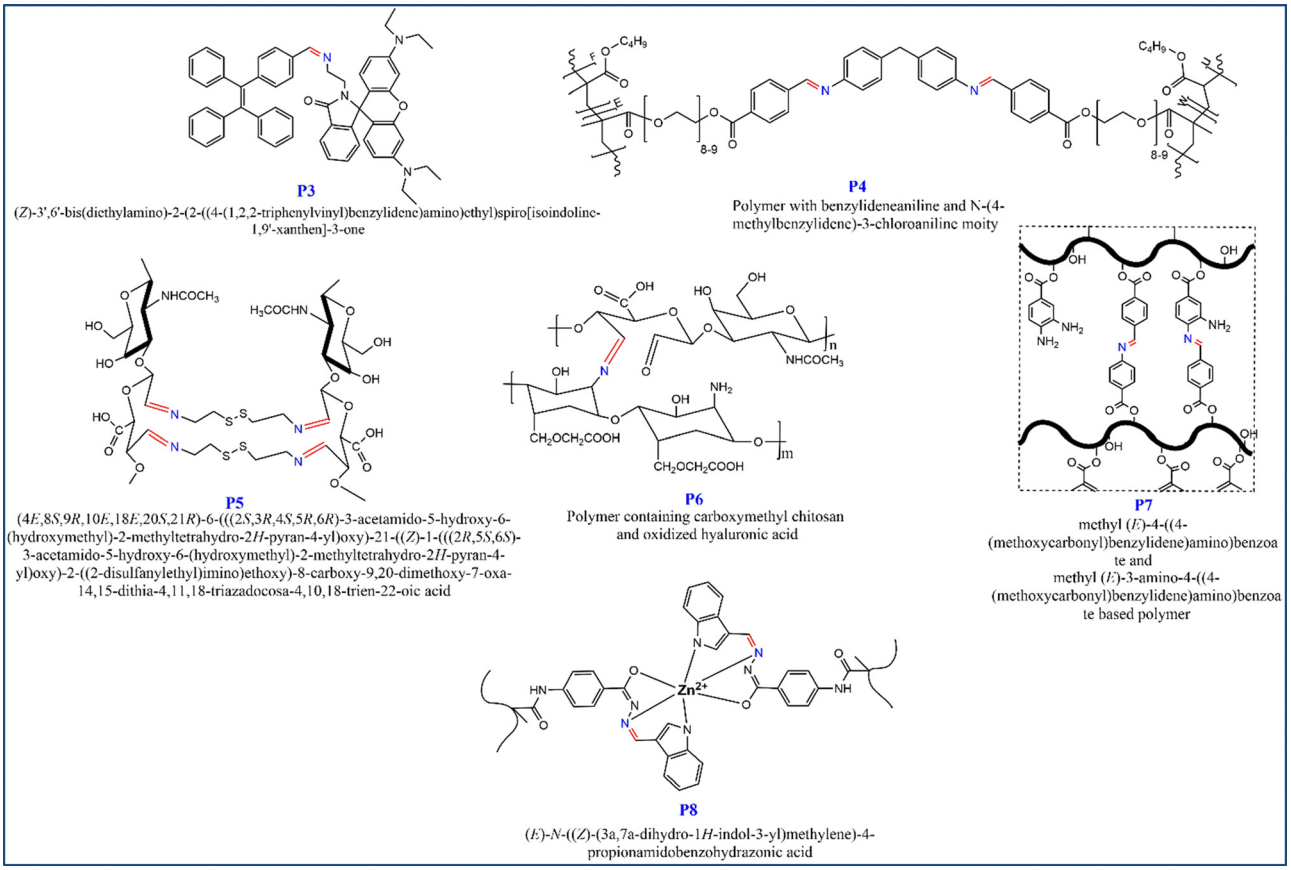

Scheme 4 Schiff base-based systems exhibiting self-healing capacity.

wide-ranging applications when coordinated with metal ions.[109–111] These complexes significantly enhanced the mechanical properties of polyacrylate hydrogels by covalently connecting polymer networks and dynamically coordinating with metal ions (**P13** and **P14**) The hydrogel, developed *via* light-triggered micellar copolymerization and Eu^{3+} coordination, could be manufactured in large dimensions (with a side length reaching 15 cm), featuring a tensile strength of 1.55 MPa and a fracture strain of 800%. Furthermore, the fluorescence intensity of the Eu-hydrogel could be modulated by adjusting the Eu^{3+} concentration, resulting in a 655% enhancement at 0.1 mol Eu^{3+}, while also displaying a fluorochromic response under mechanical stretching. This highly durable pyridine-dicarbohydrazone-based polyacrylate hydrogel, exhibiting multi–stimuli responsiveness, shows significant potential for use in information transmission, smart windows, load-bearing structures, energy-absorbing materials, and flexible wearable devices.[112] Further advancements include the development of multifunctional Schiff base-functionalized hydrogels **P15**, and its metallo-hydrogel counterpart, Zn^{2+}-**P15**. These hydrogels display tunable fluorescence, self-healing, stretchability, and shape-memory properties. They were synthesized *via* one-pot micellar copolymerization, while Zn^{2+}-**P15** is formed through metal coordination between the Schiff base ligand **P15** and Zn^{2+}, achieving a tensile strain exceeding 900%. The enhanced binding energy and crosslinking density arise from the combined effects of non-covalent interactions, including hydrophobic interactions, hydrogen bonds, and metal coordination.[113] Tang and their team advanced their research by developing a double network hydrogel (**P16**) composed of SiO_2 nanoparticles, polyacrylamide, and phytic acid doped with pyrrole. This hydrogel was utilized as a strain sensor, exhibiting a wide sensing range,

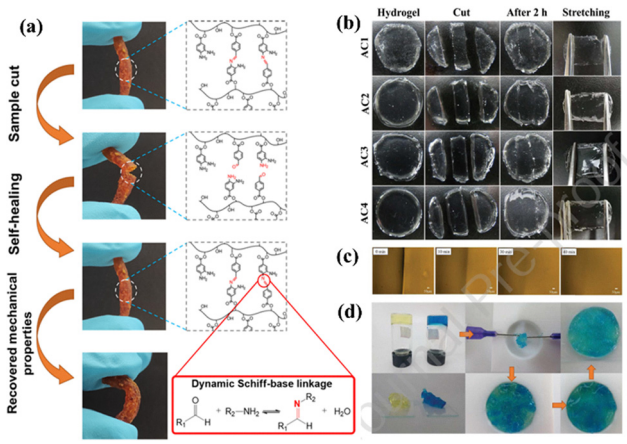

Fig. 10 (a) Self-healing mechanism (24 hour) of PVA–CHO–NH_2 polymer (**P7**) *via* Schiff base reaction; reproduced from ref. 102 with permission from Elsevier, Copyright 2022; (b) self-healing ability **P5** hydrogel induced by cutting, (c) microlevel illustration of the hydrogel at different times after the hydrogel is cut, (d) optical evidence of the self-healing process; reproduced from ref. 103 with permission from Elsevier, copyright.

exceptional adhesive properties, and stable performance under extreme conditions, including high heat and cold. Their findings revealed an impressive adhesive strength of up to 79.7 kPa, with a remarkable elongation capability of up to 1896%, even in low-temperature conditions. Additionally, the hydrogel demonstrated flame retardancy, at the surface temperature of 71 °C and after 1200 seconds of heating at 200 °C, while also offering anti-freezing properties at temperatures as low as −20 °C.[114] Multifunctional adhesive hydrogels have significant promise for use in flexible wearables, smart devices, and biomedical materials. However, creating a hydrogel that meets all these demands has remained a challenge. In 2022, this research group introduced hydrogel **P17**, which was synthesized through the copolymerization of an arginine derivative, an imidazolium salt-based ionic liquid, and acrylic acid. Notably, its real-time applications are particularly impactful due to its remarkable properties, including high transparency (85%), ultra-stretchability (2613%), elasticity (withstanding 1000% strain cycles for 10 repetitions), fatigue resistance (200 cycles at 80% compressive strain), self-healing, excellent adhesion in both air and water and electrical conductivity. The incorporation of metal ions further improved its mechanical strength, adhesion, biocompatibility, antibacterial activity, shape memory, fluorescent writing, and information transfer capabilities.[115] The creation of a physically cross-linked Schiff base fluorescent hydrogel, designated as **P18** utilized solvent exchange techniques that greatly improved the hydrogel's mechanical properties and adaptability. This hydrogel displayed a transition temperature range of 33 to 40 °C, with 33 °C being the lower critical transition temperature. The researchers investigated its shape memory properties, solvent-responsive fluorescence, and writing capabilities. This fluorescent hydrogel's extraordinary strength and durability make it attractive for use in flexible sensors, temperature-regulating materials, and anti-fatigue materials.[36] Another charge transfer hydrogel (**CTH**) is prepared by using a pyranine derivative (sodium 8-((4-vinylbenzyl)oxy)pyrene-1,3,6-trisulfonate) and viologen derivative (1-methyl-1′-(4-vinylbenzyl)-[4,4′-bipyridine] 1,1′-diium chloride iodide), as the cross-linker, and *N*-(2 hydroxy ethyl)acrylamide as the backbone monomer. The CTH provides rapid self-healing, injectability, and thermosensitivity, is good for skin adhesion, and has broad-spectrum antibacterial effects. With excellent biocompatibility and long-lasting stability, they show great potential for wound dressings.[87] Scheme 5 provides a year-wise research work summary, including the system they used for significant applications.

Similarly, rhodamine and its derivatives bridged by a Schiff base structure (**P3**), show good responses toward shearing and hydrostatic pressure, and excellent multicoloured acidichromism, as well as AIEE due to the presence of the imine group

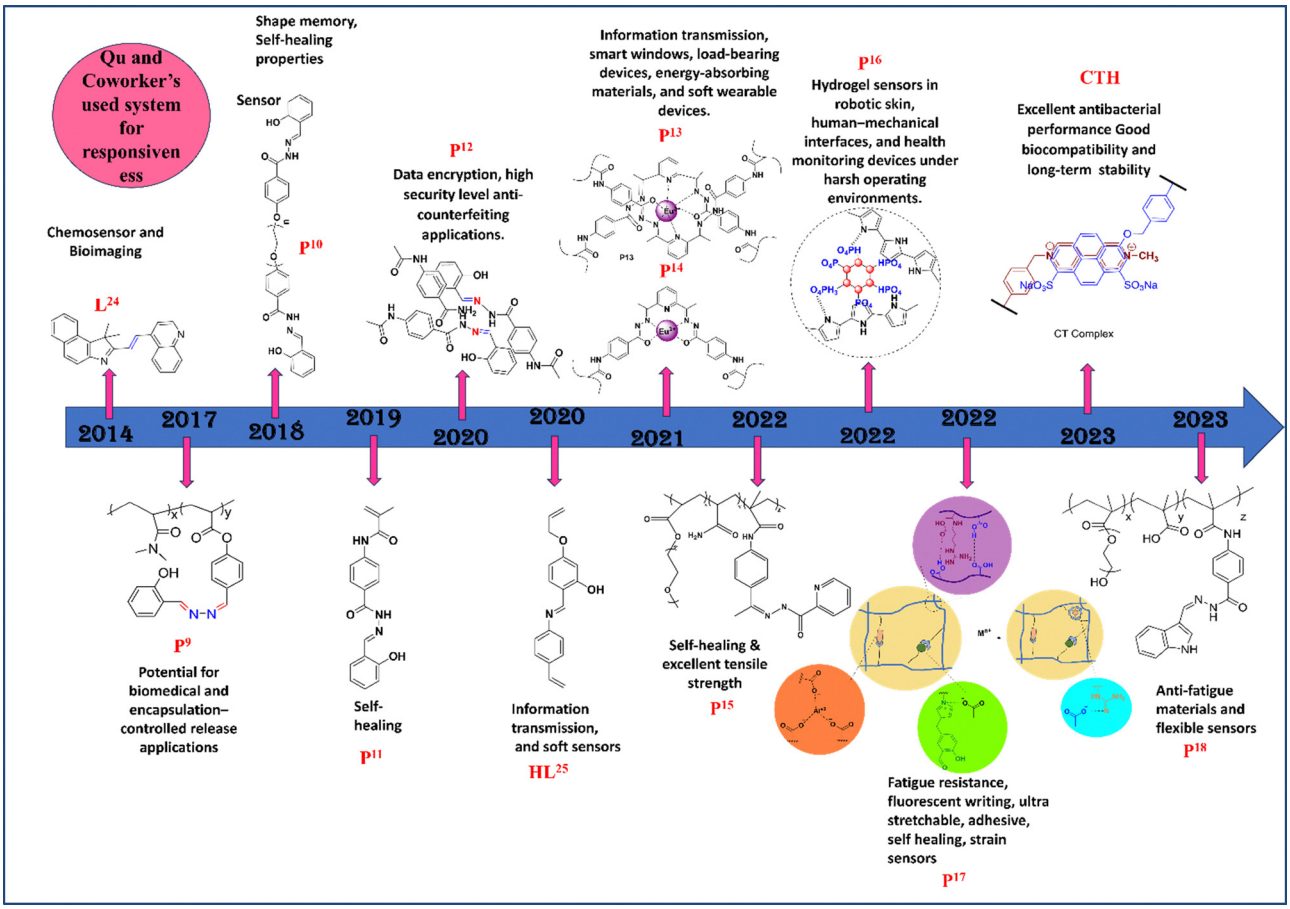

Scheme 5 Year-wise research work summary of Qu and co-worker.

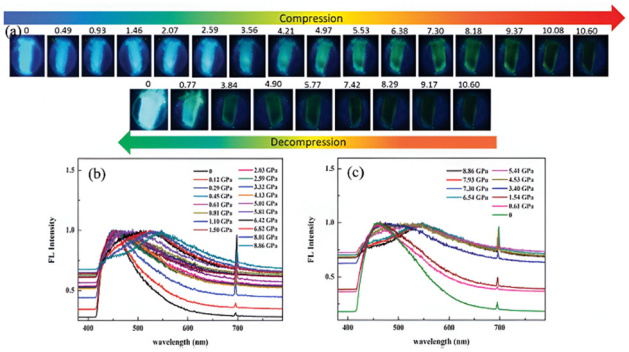

Fig. 11 (a) Fluorescence images and (b) and (c) spectra captured *in situ* at 365 nm (excitation) of a single crystal of **P3** during compression and decompression; reproduced from ref. 65 with permission from Elsevier, Copyright 2019.

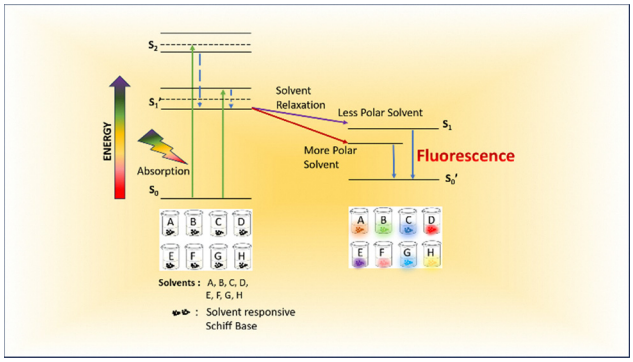

Scheme 6 Solvatochromic behaviour.

and spiro-lactam structure as well as due to the sensitivity of rhodamine towards force, acid/base and light during structural isomerization.[116] The water-induced aggregation and aggregation-suppressed nonradiative relaxation of the excited state are responsible for the enhancement in the emission property of **P3** in the THF/H_2O system upon employment of anisotropic shearing force and isotropic hydrostatic pressure. The conversion of LE emission to HLCT emission, followed by ring opening species of rhodamine lactam, accounted for the shift in colour of emission from blue (440 nm) to green (475 nm) to red (580 nm). Similarly, pressure-induced separation of HLCT, followed by emission quenching, causes the single crystal's colour to change from blue to green to dark when hydrostatic pressure is applied. Furthermore, fuming with TFA protonates both, the imine and rhodamine lactam groups, ultimately resulting in a high-contrast sequential colour shift from blue to yellow to red (Fig. 11). The ability to respond to both external force and protonation with a sequential multicolour transition makes **P3** a rare and unique dyad. Thus, understanding the various factors responsible for multicolour changes may aid in generating more facile multi–stimuli responsive fluorescent molecules.[65]

2.4 Solvatochromism

The influence that a solvent exerts on a molecule, eventually affecting its optical spectra, is known as solvatochromism. This process governs the relationship between the electronic structure of the molecule and its surroundings. When a change is made in the surroundings, the solvent eventually changes the colour emitted by the corresponding compound. Each solvent has distinct effects on the excited and ground states of any compound. A change in solvent is always accompanied by a corresponding shift in the polarity and dielectric constant of the circumambient medium. Hence, understanding the polarity of the ground and electrically excited states offers one insight into the solute's photophysical behaviour. Schiff bases and their complexes, due to the existence of keto–enol tautomerism (changes in polarity), have been extensively studied for solvatochromic behaviour [Scheme 6]. However, compounds with no tautomerism have also been shown to possess the capacity of solvatochromism due to solute–solvent interaction through the formation of non-covalent interactions.[117] Different solvent polarity characteristics can be studied to gain information about the effect of the solvent on fluorescence properties. In addition to the bipolar characteristic or polarizability of solvents, proton-donating and accepting power also play a crucial role during photoluminescence. The presence of a larger dipole moment of the singlet excited state when compared to the ground state indicates the potential of this kind of compound. ICT produces a relaxed singlet excited state, which is used to synthesize luminescent materials, non-linear optical materials, and fluorescent probes.[118] Scheme 7 exhibits various Schiff base systems with solvatochromic behaviour.

Tetraphenylethene-substituted Schiff base $\mathbf{L}^{26}$ exhibits water-induced fluorescence with a shift from Kasha's rule to anti-Kasha's rule emission. Due to this shift, an increased fluorescent quantum yield was obtained. In THF, the substituted Schiff base exhibited weak yellow-green emission following Kasha's rule. However, upon contact with water, the emission colour shifted to an intense sky blue, attributed to an unusual anti-Kasha's rule emission. The presence of an intramolecular hydrogen bond in the $\mathbf{L}^{26}$ molecule in THF increases the π electron delocalization, leading to a reduction in transition energy, which ultimately shifts the absorption peak towards longer wavelengths. This shift is attributed to the ESIPT reaction occurring due to the excited state of the keto tautomer.[119,120] However, this intense K emission band at 525 nm decreases with the increase in solvent polarity. Since this molecule is poorly soluble in water (a polar protic solvent), increasing its concentration—after being well-dissolved in THF—leads to aggregation, resulting in enhanced emission and a colour shift from weak yellow-green to intense sky blue. This process of emission change can also be explained by the fact that, in addition to water, the intramolecular H-bond breaks and intermolecular hydrogen bonds get formed between the OH group of $\mathbf{L}^{26}$ and the water molecule, which causes the dynamic emission changes (Fig. 12).[121]

Similarly, the pyrene–pyrimidine-based Schiff base ($\mathbf{L}^{27}$) has been reported to exhibit solvatochromism. This may be seen by examining the absorption spectra of $\mathbf{L}^{27}$ in various polar solvents, ranging from water to cyclohexane. A broad band with a maximum between 384 and 405 nm can be assigned to

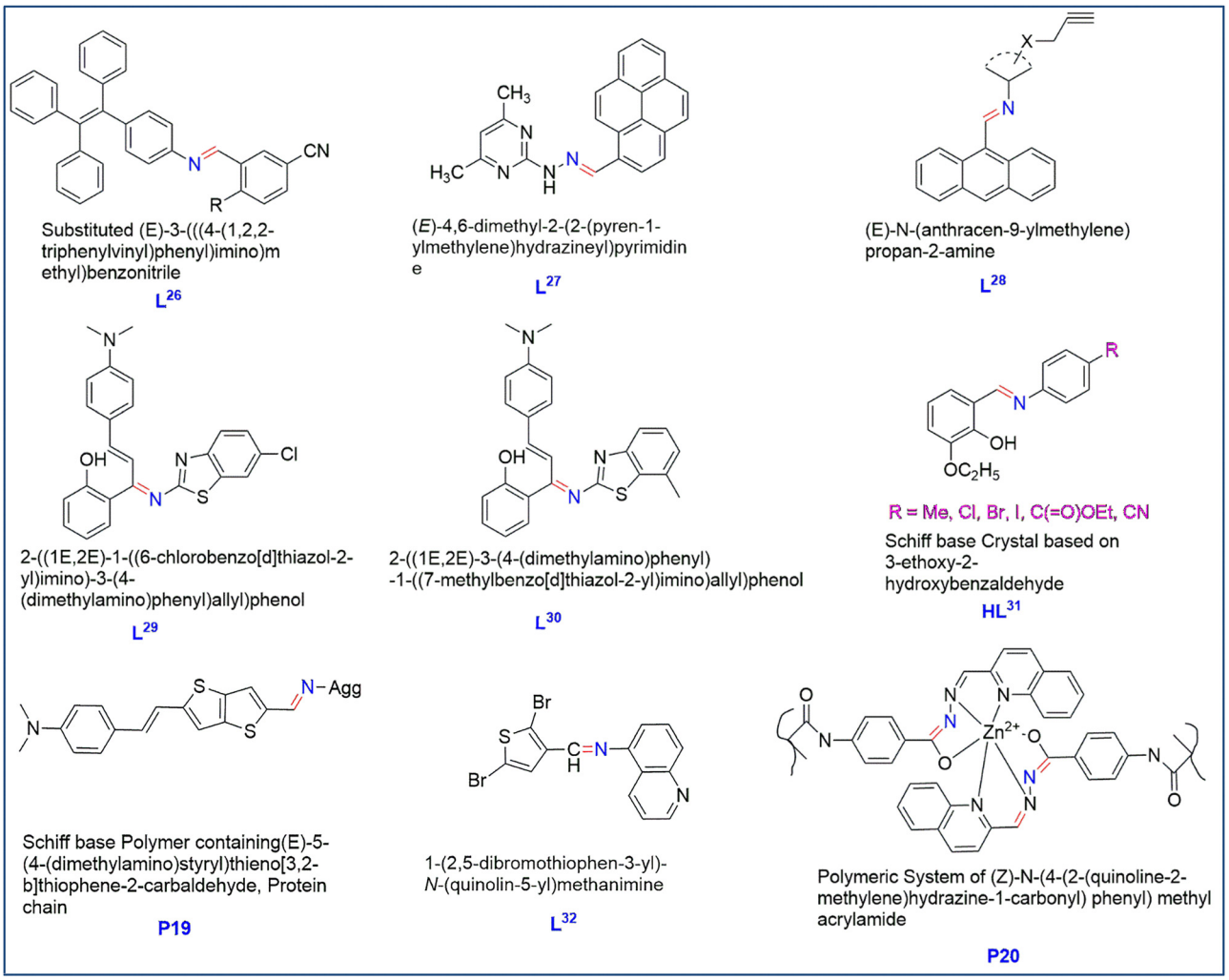

Scheme 7 Schiff base system exhibiting solvatochromic behaviour.

the p–p transition to a singly excited state (S1) of the molecule. The intensity of fluorescence decreases in non-polar solvents, whereas in polar solvents, the fluorescent intensity increases. This shift suggests that the molecule has a polar ground state. However, a more prominent red shift in the fluorescence as compared to the absorption maximum suggested the presence of a more polar emitting state in pyrene-pyrimidine-based Schiff base. This excited state gets stabilized by varying the medium from non-polar to polar, except for water and ethylene glycol in water, where strong intermolecular hydrogen bonding exists, which decreases the Stokes line.[122]

El-Nahass prepared two fluorescent probes based on Schiff bases namely 2-((1*E*,2*E*)-1-(6-chlorobenzo[*d*]thiazol-2-ylimino)-3-(4-(dimethylamino)phenyl)allyl)phenol (**L**^{29}) and 2-((1*E*,2*E*)-3-(4-(dimethylamino)phenyl)-1-(4-methylbenzo[*d*]thiazol-2-ylimino)allyl) phenol (**L**^{30}) and investigated the interaction with different solvents under normal ambient light and UV light. Under normal light, no distinguishable images appear; nevertheless, when exposed to UV light, the solution emits significant fluorescence due to polarity differences with solvents (Fig. 13). This behaviour points to the potential application of molecular probes in super-resolution fluorescence imaging.[123]

Tigineh *et al.* investigated a series of Schiff bases synthesized and examined how changes in substituents and solvents at varying concentrations influenced their absorption and emission spectra. The study focused on the UV-vis and photoluminescence characteristics of aromatic salicylideneaniline Schiff-base (**HL**^{31}) derivatives with a range of substituents, from electron-donating (*e.g.*, CH_3) to electron-withdrawing groups (*e.g.*, Cl, Br, I, C(═O)CH_3, C(═O)OC_2H_5, CN), as well as derivatives containing nitrogen within the aromatic ring. These derivatives were tested in solvents with diverse dielectric constants, including *n*-hexane, toluene, ethyl acetate, THF, ethanol, and methanol. According to the photoluminescence analysis results, substituents in a particular high dielectric constant solvent have no discernible effect on the fluorescence spectra of **HL**^{31}; however, with a change in substituent, the position, intensity, and shape of the fluorescence spectra in a given reduced dielectric constant solvent alter slightly. However, the photoluminescence study confirmed that ESIPT exists in solvents with lower dielectric constants. In solvents with a high dielectric constant, the emission spectra displayed a single band in the visible area of electromagnetic radiation; in solvents with a

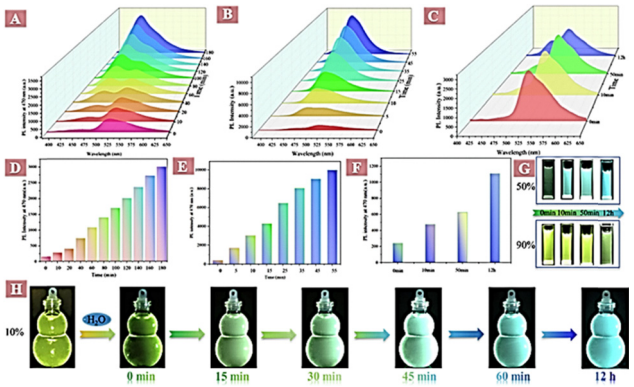

Fig. 12 Changes in fluorescence spectra and intensity of L^{26} in THF/H_2O at 470 nm in THF/H_2O mixtures with different water fractions of 10% (A) and (D), and 50% (B) and (E), respectively. (G) Changes in emission images of L^{26} with time for the 50% and 90% samples. (H) The emission images change of L^{26} (10^{-4} M in 10% THF/H_2O) mixtures with different time intervals at an excitation wavelength of 370 nm, and excitation wavelength of 370 nm UV; reproduced from ref. 121 with permission from Elsevier, Copyright 2021.

lower dielectric constant, they were present in the bimodal emission spectrum in the same region.[124]

Optoelectronic analysis of quinoline-based Schiff base (L^{32}) revealed an impressive AIEE effect, resulting in a 21-times increase in fluorescence intensity at a THF ratio of 80 : 20, as confirmed by dynamic light scattering (DLS) studies. Additionally, it demonstrated exceptional selectivity and sensitivity in detecting Co^{2+} and Mg^{2+} ions among various heavy metals, with detection limits of 4.5 μM and 5.7 μM for Mg^{2+} and Co^{2+}, respectively. This makes QSB a promising candidate for fluorescence sensing and ion detection applications.[125]

In addition, Schiff bases based on polymeric protein chains, thiophene, hydroxybenzaldehyde, and polymeric systems of (*Z*)-*N*-(4-(2-(quinoline-2-methylene)hydrazine-1-carbonyl) phenyl) methyl acrylamide, *etc.*, exhibiting solvatochromic behaviour, are further discussed with their applications in Section 5 of this review.

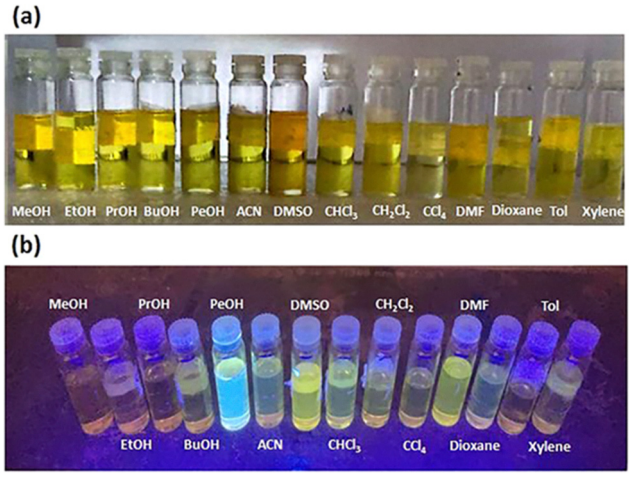

Fig. 13 Fluorescence images of Schiff base (L^{30}) in different solvents: (a) Normal light (no emission), (b) upon UV radiation (emission wavelength, λ_{ex} = 366 nm) at room temperature; reproduced from ref. 123 with permission from Elsevier, Copyright 2024.

3. Multi–stimuli responsive behaviour

3.1 Mechanochromic–acidochromic

The complex's ability to exhibit acidochromism also depends on its crystallinity, where protonation and deprotonation play key roles in controlling luminescence through solvent changes. Overall, these complexes open exciting possibilities in responsive luminescent materials. In Fig. 14, Schiff base complex HL^1 exhibits blue emission when exposed to a 365 nm UV lamp. The emission peak is centred at 457 nm. The emission peak red-shifted to 545 nm and turned green after being ground with a pestle and mortar, displaying high-contrast mechanochromic luminescence. The complex's ability to exhibit acidochromism also depends on its crystallinity, where protonation and deprotonation play key roles in controlling luminescence through solvent changes. Overall, these complexes offer exciting possibilities in responsive luminescent materials.[61]

However, the formation of ligands on the surface by decomposition of the complex in the reaction with acid and the self-absorption effect also shifts the emission of acidochromic luminescence.[126]

Rhodamine blue and tetraphenylethene-based Schiff base **P3** show exceptional proton sensitivity, changing colours sequentially in the solid state from blue/green to yellow and then to red when exposed to TFA fumes (Fig. 15). Initially blue, the powder turns yellow with TFA and then red after TFA is removed. Spectral analysis reveals that new emission and absorption bands form and shift during this process, linked to the protonation and ring-opening of rhodamine lactam. The colour reverts from yellow to blue when fumed with triethylamine (TEA), highlighting the unstable nature of imine protonation and its role in triggering the rhodamine lactam ring-opening reaction.[65]

3.2 Mechanochromic–photochromic

Schiff bases with salicylaldehyde hydrazone ligand (H_2L^{11}) (Fig. 16(a)), due to their excellent luminescence properties and multiple coordination sites, have emerged as potential multi-responsive materials for various applications. In this regard, Zn(II) complex (b, c and d) in Fig. 16 based on

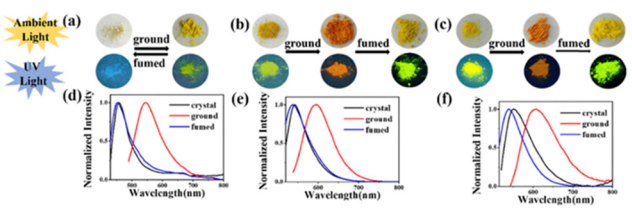

Fig. 14 Images and fluorescence spectra of HL^1 (a) and (d), 1-Zn-complex of HL^1 (b) and (e), and 1-THF (c) and (f) under ambient light and UV irradiation at 365 nm under different conditions; reproduced from ref. 61 with permission from ACS, Copyright 2022.

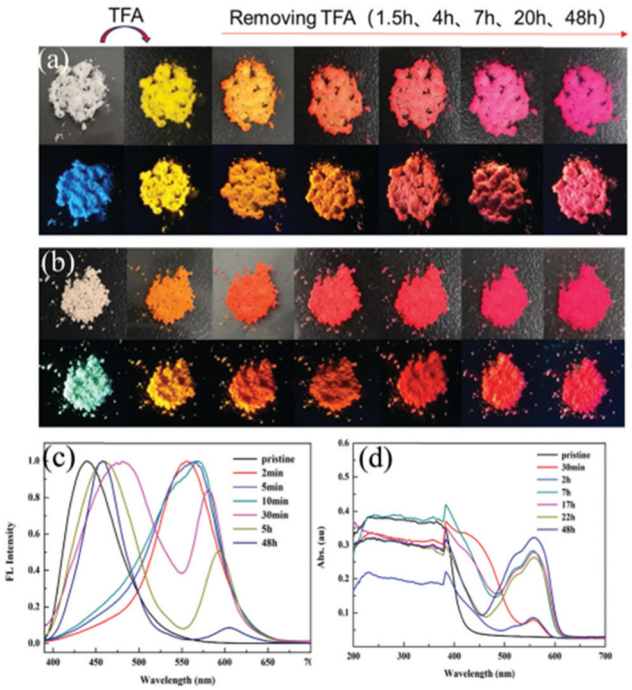

Fig. 15 Image of colour change in **P3** for (a) the original powder and (b) the ground powder fumed with TFA and after withdrawing TFA; (c) fluorescence and (d) absorption spectra of the original powder fumed with TFA and after withdrawing TFA; reproduced from ref. 65 with permission from RSC, Copyright 2019.

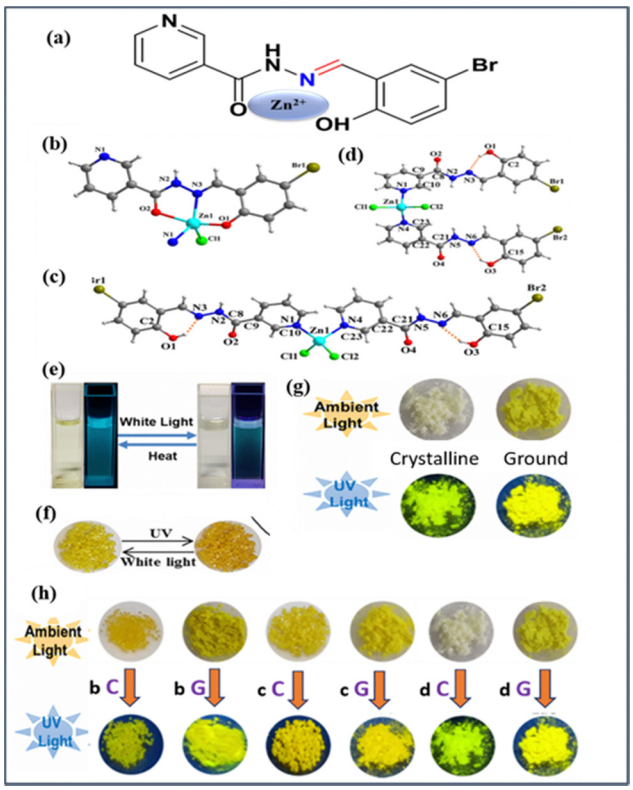

Fig. 16 (a) Chemical and (b), (c), (d) molecular structure of H_2L^{11} and complex synthesized using salicylaldehyde hydrazone ligand, respectively. (e) & (f) Photochromism shown by complex (b) & (c). (g) Mechanochromic luminescence property displayed by complex (d). (h) Photographs showing mechanochromic properties of complexes (b), (c) and (d) under ambient light and 365 nm UV light; reproduced from ref. 127 with permission from ACS, Copyright 2023.

salicylaldehyde hydrazone with an O,N,O-tridentate coordination mode, with different conformation and coordination modes synthesized using different ratios of solvent and reactant but using the same precursors (nicotinic hydrazide and 5-bromosalicylaldehyde) were reported possessing photochromic and mechanochromic properties respectively. While complexes b and c both displayed photochromic and photoluminescence properties in solution and crystal state, respectively. Only complex a is capable of reversible and self-recoverable photochromism. This stimuli-responsive behaviour can be attributed to the configuration eversion, and ESIPT process, depending on the intramolecular hydrogen bonds, for complex a and electron transfer and generation of single-electron free radicals upon UV irradiation. The third complex *i.e.*, b, exhibited mechanochromic luminescence properties. The conversion from a crystalline to an amorphous state (C for crystalline and G for ground or amorphous) upon grinding can be attributed to the disruption of intermolecular interactions, which is responsible for the observed stimuli-responsive behaviour. In addition (Fig. 16(g) and (h)), complex b on providing force or vapour can also undergo crystal phase transformation to form c.[127] Continuing their work with Zn(II) complexes based on salicylaldehyde hydrazone (Fig. 17(a)), Zheng *et al.* reported the synthesis of three different complexes (b, c and d) drawn in Fig. 17 *via* self-assembly of 3-hydroxy-2-naphthoic acid hydrazide, salicylaldehyde derivatives, pyridine, and Zn(II). While complex b and d are capable of showing reversible mechanochromism in the solid state upon grinding and fuming due to crystalline to amorphous phase transformation (Fig. 17(e) and (f)), complex b can also undergo crystal phase transformation to form c. In addition, complex b and d also displayed reversible photochromism on UV illumination in the solid state (Fig. 17(h) and (i)). The induction of electron transfer from the hydroxyl oxygen to the pyridine molecule upon UV exposure generates radicals, which might be responsible for the photochromic behaviour of both the complexes in the solid state. A photochromic response ascribed to the configuration inversion was also recorded in solution for complexes b and d (Fig. 17(g)), with a reversible phenomenon for only b, due to the occurrence of steric hindrance in complex d. The generation of these salicylaldehyde hydrazone Zn(II) complexes, displaying both mechanochromic as well as photochromic luminescence behaviour, shedding light on the mechanism of MCL and photochromism in solution as well as the solid state can emerge as promising multi-stimuli responsive materials.[128]

3.2 Stress–strain and thermoresponsive properties

Lu *et al.* synthesized the **P18** hydrogel by modifying a hydrophobic Schiff base monomer with polyethylene glycol (PEG) and methacrylic acid (MAA), resulting in excellent mechanical properties and temperature-responsive behaviour. When

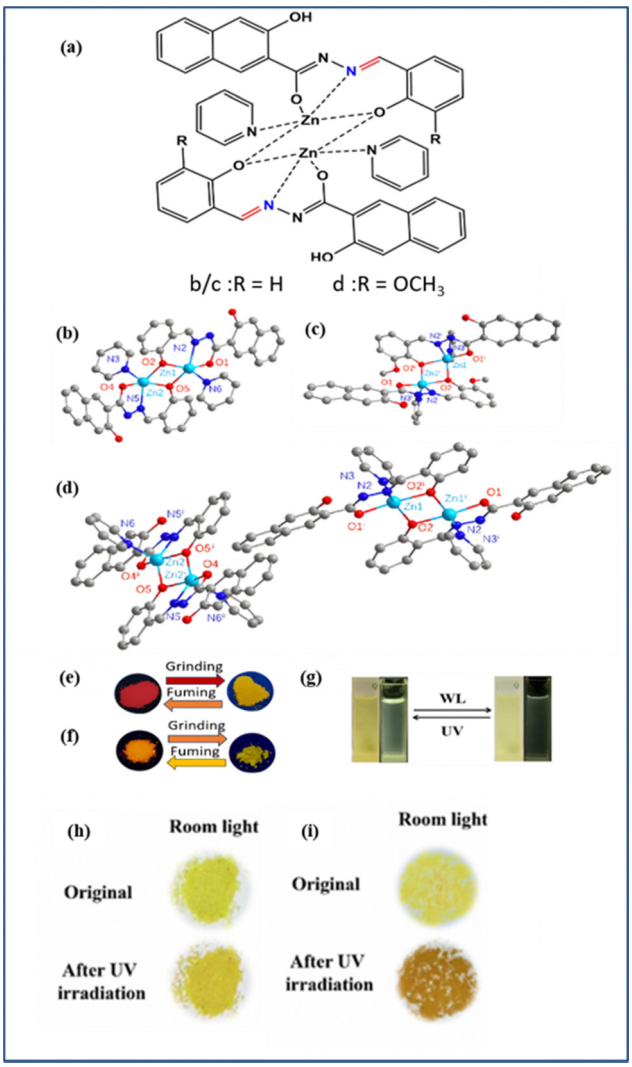

Fig. 17 (a) Schematic diagram of complex (b), (c), and (d). (b), (c), and (d) Molecular structures of Zn(II) complexes based on salicylaldehyde. (e) & (f) Photographs showing mechanochromism in complex (b) and (d). (g) A reversible photochromic response shown by complex (b). (h) & (i) Complex (b) & (d) showing reversible photochromism under UV illumination in the solid state; reproduced from ref. 128 with permission from ACS, Copyright 2025.

complexed with Zn^{2+}, it became tougher and exhibited increased fluorescence and antibacterial properties. The presence of multiple hydrogen bonds in PEG was one of the major factors governing the thermoresponsive behaviour of the hydrogel. Due to the high fluorescence behaviour of this hydrogel, it can be utilized in anti-fatigue materials, temperature control materials, and flexible sensors. Fig. 18 shows the loading–unloading tensile strength test with different IHPMA contents. The hysteresis loop ranging from 0.08 to 0.25 MJ m^{-3} suggests that the hydrophobic association points to the hydrogel gradually break down. The energy dissipation ratio being less than 13.6% indicates that the **P18** hydrogel exhibits good recovery properties. However, the tensile stress at 80% strain in the second loading–unloading cycle is noticeably higher than in the first cycle (Fig. 18(a) and (b)). Additionally, as shown in Fig. 18(c) and (d), the hydrogel exhibits 87% transmittance at

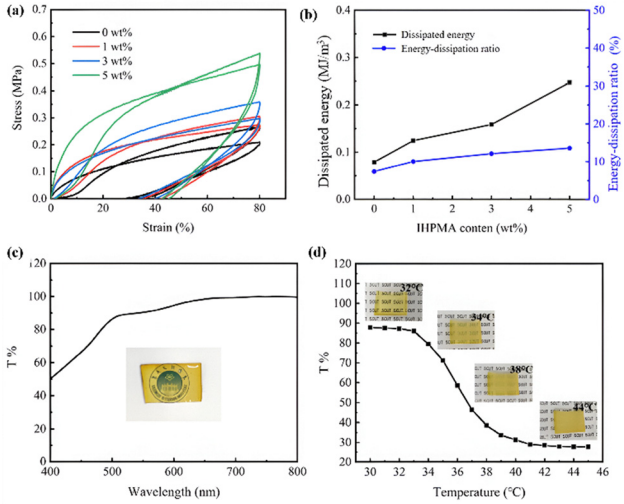

Fig. 18 (a) **P18** showing a continuous loading–unloading cycle, (b) changes in dissipation energy, (c) transmittance plots and optical photographs of **P18** hydrogel at room temperature, and (d) temperature-transmittance change curves; reproduced from ref. 36 with permission from Wiley, Copyright 2023.

500 nm at room temperature, allowing the school emblem pattern to be visible through the hydrogel, indicating excellent transparency. As shown in Fig. 18(d), the transmittance begins to decrease above 33 °C, dropping to 27% beyond 40 °C. At 44 °C, the hydrogel becomes mostly opaque, making it difficult to see letters through it.[36]

3.3 Thermo-pH responsiveness

Abdelaty produced 2-((dimethylamino)methyl-4-formyl-6-methoxyphenyl acrylate (**P2**) and used it in combination with *N*-isopropyl acrylamide, **P2**, and styrene in varied ratios to create three thermo-pH responsive terpolymers. Furthermore, they investigated how changes in the hydrophilic and hydrophobic groups in polymer chains affected contact angles in pH and water solutions, concluding that the lowest contact angle exhibited the highest hydrophilicity. Furthermore, in the strongest basic solution, the anionic carboxylate ion at $\theta = 76°$ exhibited the highest degree of hydrophilicity. The presence of distinct hydrophilic/hydrophobic groups influenced the transition temperature of the produced terpolymers because, in an aqueous solution, they were responsible for the following increase and reduction in hydrogen bonding (Fig. 19). Another term, cloud point, can be used for the justification of this phenomenon. The results showed that increasing the amount of **P2** in the main polymer chain raises the transition temperatures and cloud points. This indicates that the hydrophilic groups, formed by the cationic protonation of tertiary amine groups in the polymer solution, dominate. This also improves hydrogen bond interactions between the polymer chain and the aqueous solution, thereby enhancing the hydrophilicity of the polymer solution.[129]

3.4 Thermo-vapochromic responsiveness

Gaeta *et al.* reported the Schiff-base complex with Zn metal **ML**[19] exhibiting peculiar thermo- and vapochromic properties.

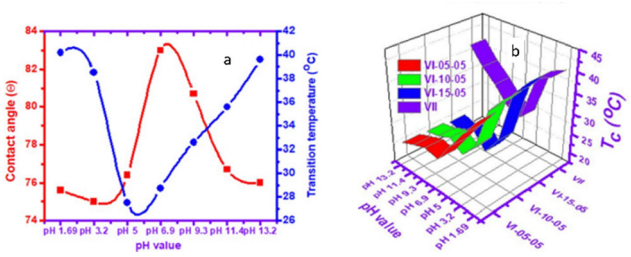

Fig. 19 The change in transition temperature ($T_{c,s}$) and contact angles (θ)° *via* the pH contact angles (θ)° against pH changes; reproduced from ref. 129 with permission from Springer, Copyright 2023.

The reversible desorption/adsorption of a single lattice water molecule is the uncommon cause of this intense thermochromism associated with a phase transition in the solid complex generated in air or by solvent evaporation from their THF solutions.[130]

In contrast, the anhydrous solid, obtained from THF solutions of the complex by evaporating the solvent under anhydrous conditions, behaves quite otherwise. It does not absorb water, lacks thermochromism, and displays distinct vapochromic properties. To detect volatile organic molecules with Lewis basicity, the anhydrous solid or similar cast films on glass or paper substrates can be utilized. In both cases, distinct vapochromism can be achieved upon exposure to vapours of numerous volatile species, featuring precisely defined optical absorptions and noticeable colour changes visible to the naked eye, which also allow for the discrimination of primary aliphatic amines. The solid obtained in air and the anhydrous solid, as well as the corresponding cast films following exposure to pyridine vapours, exhibit the vapochromic characteristic, which

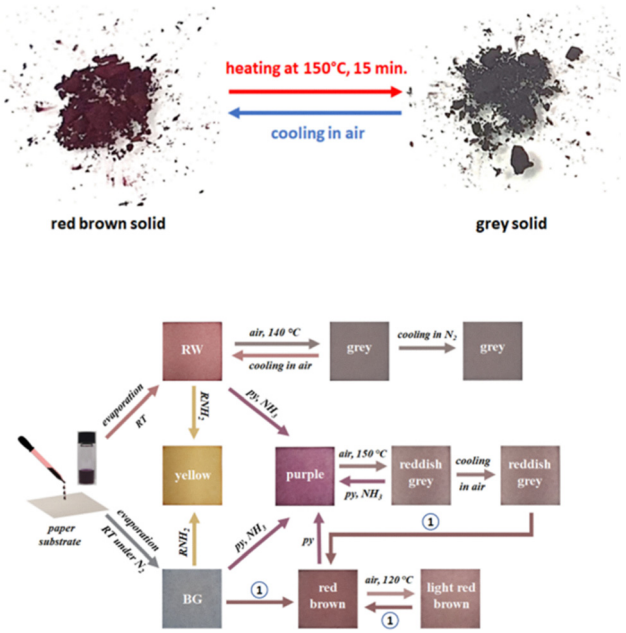

Fig. 20 Thermo and vapochromic behaviour shown by paper substrate containing a **ML**[19] complex; reproduced from ref. 130 with permission from ACS, Copyright 2024.

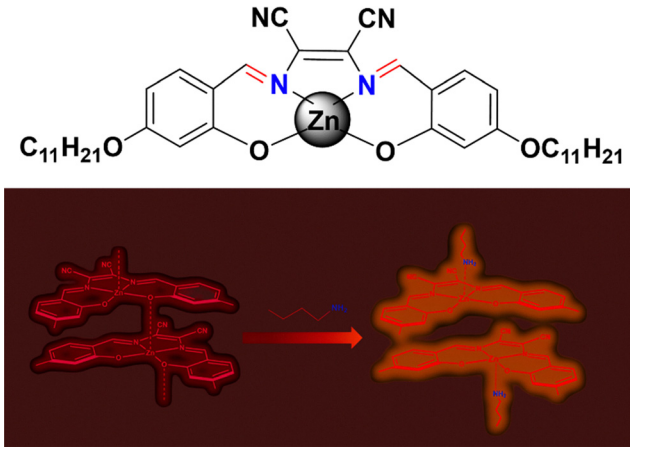

Fig. 21 Vapochromic behaviour shown by **ML**[12] for *n*-butylamine; reproduced from ref. 131 with permission from Elsevier, Copyright 2024.

involves the creation of stable, stoichiometric adducts (Fig. 20).[130] In an attempt to develop a suitable material for sensing volatile Lewis bases, Zn(salen)-type complexes have emerged as promising, low-cost, stimuli-responsive materials. Exhibiting reversible vapochromism or vapoluminescence on exposure to vapours of a volatile compound, a novel Lewis acidic Zn(salen)-type complex with **ML**[12] was developed for the detection of *n*-butylamine (BA) vapours. The formation of stable monomeric adducts with significant differences in photophysical properties compared with the starting aggregates can be attributed to the vapochromic behaviour of the complex. The simple, reusable, and economic paper-based sensor developed using this complex showed high selectivity and sensitivity towards the detection of *n*-butylamine vapours with respect to various classes of VOCs under static conditions (Fig. 21).[131]

4. Mechanisms and modeling of responsiveness

Compounds based on Schiff bases are well-known for their dynamic covalent structure, which allows them to react to a variety of stimuli. Schiff bases are characterised by the reversible creation and cleavage of imine (C═N) bonds, which is the main mechanism of responsiveness in these compounds. For instance, an imine can hydrolyze in either an acidic or basic environment, cleaving the C═N bond into its parent amine and a carbonyl molecule. Higher temperatures cause cleavage due to increased bond tension and enhanced molecular mobility. Reversible changes in the structure, solubility, or aggregation states can result from the stabilization or destabilization of the imine bond by solubility effects. Coordination bonding in Schiff bases can alter the electronic structure of the molecule, leading to colour variations. Other mechanisms, such as the ESIPT process, require the transfer of protons within an excited molecule, which forms a tautomer that emits fluorescence at a different wavelength. Strong fluorescence characteristics are displayed by the AIE mechanism when it aggregates. In such

cases, non-radiative relaxation pathways are suppressed and fluorescence is enhanced by the limitation of intramolecular rotation and vibration in the aggregated state. The ICT process is based on a substantial shift in the electronic charge of a molecule upon stimulation.

Density functional theory (DFT) stands out as a powerful tool in modeling and simulating the dynamic, stimuli-responsive behaviour of Schiff bases. By providing a deep computational insight into their electronic structures and molecular properties, DFT allows us to predict how these compounds react to various external stimuli, including shifts in pH, temperature, light, solvent environments, and even interactions with ions. It offers a detailed understanding of the electronic characteristics of Schiff bases—like the frontier molecular orbitals (HOMO and LUMO), their energy levels, and the electron density distribution—all crucial for explaining how these molecules respond to different external triggers. DFT further sheds light on the relative stability of various molecular forms, such as different conformations with dihedral angles, tautomers, and isomers, by calculating the total energy under diverse conditions. Additionally, it maps out charge distributions and dipole moments, revealing how Schiff bases might behave in polar *versus* non-polar solvents. Since Schiff bases often form complexes with metal ions, DFT can also predict key details such as binding sites, coordination geometry, and binding energies, which are essential for understanding their reactivity. The insights from these calculations are invaluable for designing and tuning Schiff bases for specific applications, from smart materials to sensors.[33,56,57,132–134] Different configurations of intermolecular interactions provide precise mechanisms among molecules.[135] Here, some mechanisms and DFT studies have been provided for a deeper understanding of the multi–stimuli behaviour of Schiff bases.

4.1 ESIPT process

If the molecules undergo keto–enol tautomerization in the presence of a light photon, the proton transfer mechanism is referred to as excited-state intramolecular proton transfer (ESIPT). Between the keto and enol forms, a four-step photoisomerization process is involved[136,137] (Scheme 8). Intramolecular hydrogen bonds between a proton acceptor and a proton donor can exhibit ESIPT behaviour, a proton donor can be hydroxyl or amine, and a proton acceptor can be carbonyl or imine.[138] When the molecule's enol form is excited by photoexcitation, proton transfer or reshifting occurs on a high-speed time scale between the proton donor and acceptor, resulting in the generation of the keto form. This excited keto form emits light and transitions back to its

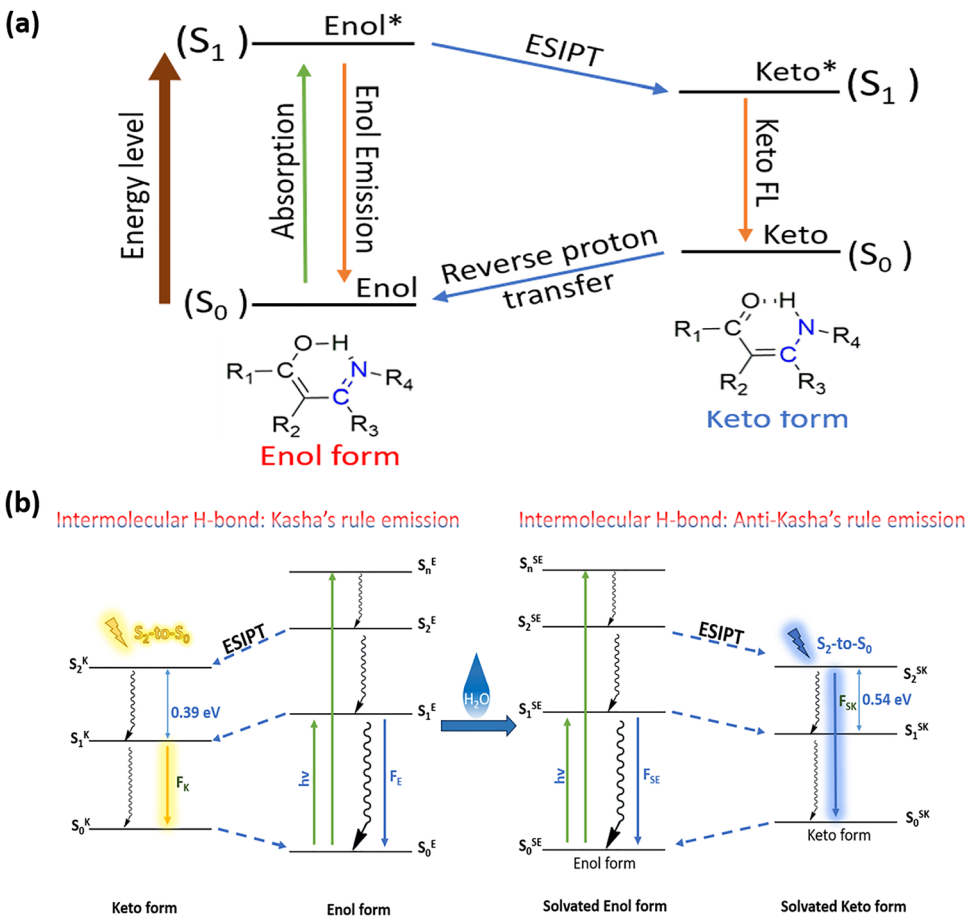

Scheme 8 (a) Schematic representation of the four-level ESIPT process. (b) Possible mechanism for the dynamic stimuli-responsive fluorescence switch, following Kasha and Anti-kasha's rule involving in intermolecular H-bond for solvated L26, respectively.[121]

ground state, where it then converts back to the enol form through a thermal reverse proton transfer process.[139] A significant Stokes shift is produced by the photochemical ESIPT process, which yields a tautomer with an electronic structure (keto form) different from the initial excited state (enol form).[140–142] This reduces the tendency for self-absorption and increases the quantum efficiency. The entire visible spectrum can be covered by the broad, controllable dual emissions of ESIPT fluorophores, resulting in the production of white light.[143,144] Temperature, pH, and solvent polarity are all potent external stimulators that interfere with proton transfer and cause significant changes in photophysical characteristics.[124,138,145–152] Various kinds of intramolecular H-bond forming core units, such as salicylic acid, flavones, benzophenones, benzimidazole, benzoxazole, coumarins, quinolines *etc.* have been studied for building efficient ESIPT fluorescent compounds.[153–164] Shekhovtsov *et al.* investigated the solvent and substituent as control factors for the ESIPT process in 2-(2′-hydroxyphenyl)benzimidazoles (HBI). Three major outcomes came into existence: (1) the ability of a solvent to form strong O–H···O hydrogen bonds suppresses ESIPT and promotes the emission of the enol form, (2) substituents with a strong –I effect, when positioned ortho to the hydroxy group, stabilize the keto form, (3) twisted intramolecular charge transfer is unfavorable in HBI, resulting in moderate to high photoluminescence quantum yields.[165] Scheme 8 represents all levels of the photophysical process. The tetraphenylethene-substituted Schiff base (**L**^{26}) has shown water-induced fluorescence with a shift from Kasha's rule to anti-Kasha's rule emission. An amplified fluorescent quantum yield accompanied this. In THF, the substituted Schiff base emitted weak yellow-green following Kasha's rule, but when it came into contact with water, the emission colour changed to bright sky blue due to unexpected anti-Kasha's emission. The presence of an intramolecular hydrogen bond in **L**^{26} molecule in THF increases π-electron delocalization, leading to a decrease in transition energy, which ultimately shifts the absorption peak towards longer wavelengths (Scheme 8). This shift is attributed to the ESIPT reaction occurring due to the excited state of the keto tautomer.[121]

4.2 AIE mechanism

A unique fluorescence phenomenon known as ''aggregation-induced emission'' (AIE) occurs when a specific type of molecule produces higher fluorescence when aggregated, but very weak fluorescence in solution.[6,166,167] The AIE feature of organic luminescent materials has demonstrated significant promise in several applications, such as light-emitting diodes,[168] photodynamic treatment,[169] fluorescent probes,[170] and so on. This mechanism can be understood with the help of various spectroscopic techniques such as NMR, DFT, IR, SEM, *etc.* The free rotation along the C–C bond in one form can result in its non-emissive nature by non-radiative deactivation in one solvent, whereas in another solvent, where the polarity of compounds shifts, it can result in the formation of aggregates. This aggregation can be accompanied by tautomerization, which produces fluorescence spectra.[25] AIE-active compounds have a highly twisted skeleton with rotatable aryl units, which results in loosely packed crystal structures. These structures can be easily disrupted by mechanical stimuli, leading to a change in the emission colour. The presence of the D–A structure in the extended π-conjugated molecules is crucial for organic dyes to show MFC characteristics.[171,172] The spectroscopic and characterization studies can help understand the mechanism for the generation of bright luminescent aggregates. NMR and DFT studies indicate that **HL**^{9} exists in a bent benzenoid form in solution, while IR and single-crystal data show a planar quinonoid form in the solid state. SEM images at varying water fractions support these findings. In acetonitrile, **HL**^{9} remains non-emissive due to free rotation along the C–C bond. Adding water alters the solution's polarity, leading to aggregation of molecules. The quinonoid form, more stable in the solid or aggregated state, forms through simultaneous aggregation and tautomerization. Though this planar form is less conjugated, it is more emissive due to restricted C=C bond rotation within its rigid structure (Fig. 22).[25] The AIE mechanism is well explained using Fig. 23.

4.3 Dynamic bond and bond flexibility

One of the most popular and extensively employed methods for synthesizing materials containing dynamic C=N imine (and imine-type) bonds, which can be more reversible and responsive in comparison to other dynamic covalent linkages such as addition (*e.g.*, Diels–Alder cycloaddition) and reversible exchange (*e.g.*, transesterification) reactions, is the Schiff base reaction. The Schiff base reaction involves the formation of C=N bonds (*e.g.*, imines, hydrazones, oximes by combining a carbonyl compound) (less reactive ketones or aldehydes) with amino-containing reactants (*e.g.*, hydrazine, primary amines, hydrazine).[21] Among these new bonds, imine bonds are more sensitive towards pH due to their lower chemical stability in aqueous medium, and thus can hydrolyze back to the reactant. This high sensitivity towards pH makes the imine linkage more responsive to stimuli. Hence, over the years, dynamic Schiff base linkages have gained significant attention for the fabrication of imine based self-healing material containing both natural as well as synthetic polymers such as includes chondroitin sulfate,[173] hyaluronic acid,[103] dextran,[174] xanthan gum,[175,176] alginate,[177] micro- or nanocrystalline cellulose,[177] chitosan,[178,179] and its derivatives (polysaccharides), as well as gelatin[180] and collagen[181] polypeptides,[182] and benzaldehyde-modified poly(ethylene glycols) *etc.*

4.4 ESIPT-induced AIE properties

SAs, Schiff bases derived from salicylaldehyde and aniline derivatives are notable for their photochromic and thermochromic capabilities, with colour changes caused by enol–keto tautomerism, which includes *cis–trans* isomerization as well as protonation.[183–186] Various publications demonstrate the AIE mechanism of SAs for thermo- and photochromic behaviour. Also, TPE, known for its twisted molecular conformation and strong aggregation-induced emission, is widely utilized in designing stimuli-responsive materials.[187] Thus, incorporation of TPE into salicylideneanilines (SAs), an AIE active molecule,

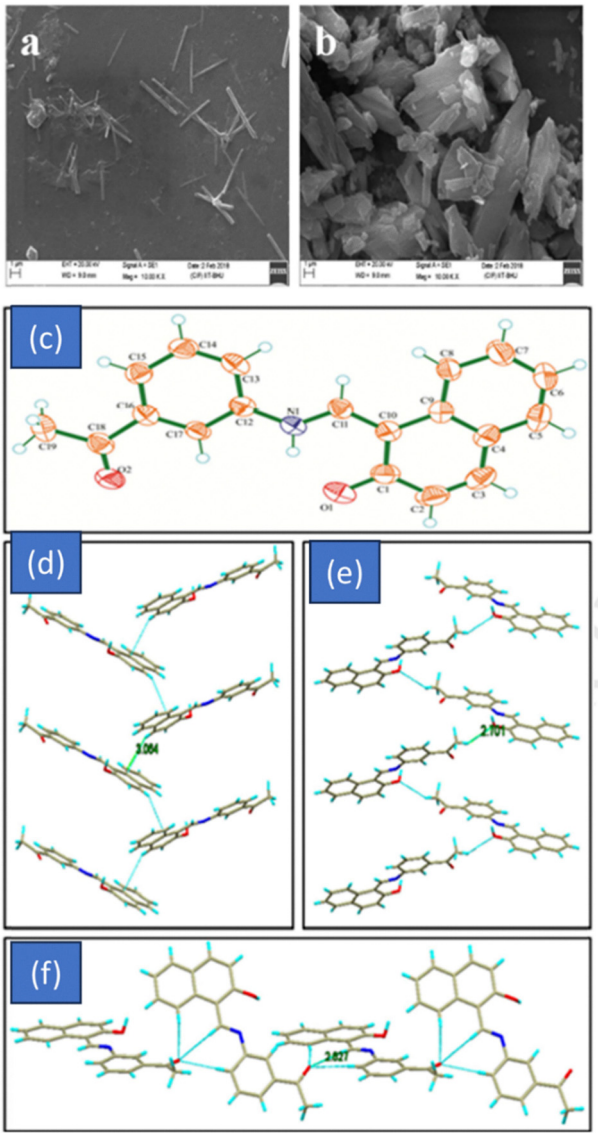

Fig. 22 SEM image of **HL**[9] (20 μM) showing aggregates in different acetonitrile–water mixtures (a) f_w = 70% and (b) f_w = 90%. (a) ORTEP diagram of **HL**[9] with ellipsoid of 30% probability. Crystal packing in the **HL**[9] molecule (b) showing C–H···π interactions and (c) and (d) showing C–H···O interactions; reproduced from ref. 25 with permission from Elsevier, Copyright 2019.

results in the occurrence of excited-state intramolecular proton transfer (ESIPT) along with AIE, resulting in distinguished photochromic behaviour in the solid state.[188,189] The excited-state intramolecular proton transfer-induced AIE can be enabled by suppressing *cis*-to-*trans* isomerization by exploiting the relatively compact crystal packing and polymorphic behaviour of **HL**[20]'s, thus causing an efficient thermochromism. The thermochromic behaviour of solid-state **HL**[20] is caused by a two-step isomerisation process involving the enol isomer and the *cis*- and twisted *cis*-keto isomers, according to theoretical calculations. The chromic transitions could be caused by the reversible interconversion of different twisted *cis*-keto forms during the heat isomerisation process.[190]

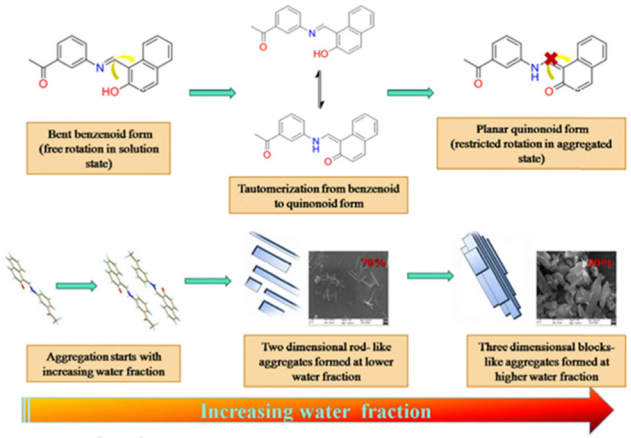

Fig. 23 Proposed mechanism of aggregation-induced emission; reproduced from ref. 25 with permission from Elsevier, Copyright 2019.

HL[20], having a TPE moiety, is twisted with large torsion angles (48°–53°) due to steric hindrance. The two phenyl rings joined by a C–N bond have a dihedral angle of 27.33° (Fig. 24(a) and (b)). The intramolecular hydrogen bond (O–H–N, 1.893 Å) facilitates enol–keto tautomerism from the OH group to the nitrogen atom, leading to ESIPT emission.[191] Along the *c* axis, staggered parallel salicylaldehyde groups (head to head) and TPE groups (tail to tail) join neighboring molecules to form a symmetrical one-dimensional structure like a goldfish. Intermolecular interactions between adjacent TPE moieties along the *b* axis (distances of 4.507 and 5.045 Å) allow for the tight packing of molecules in the crystal structure (Fig. 24(c)). These interactions also prevented the free rotation of TPE's benzene ring and significantly accelerated the radiative decay of the excited state.[192] In the meantime, adjacent salicylaldehyde groups adopted slipped π–π stacking, resulting in weak π···π

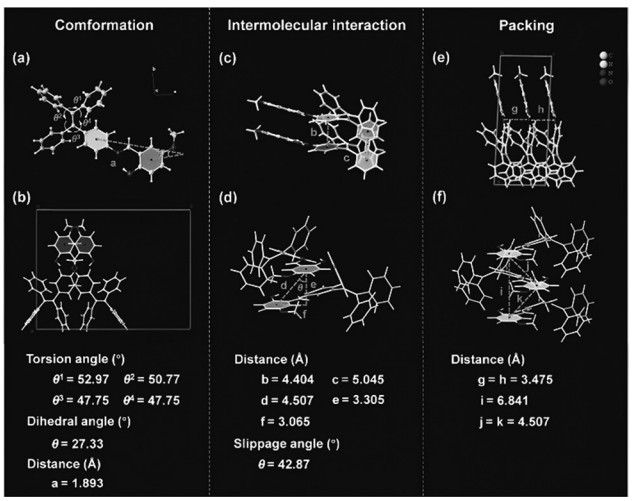

Fig. 24 (a) and (b) Single-crystal structure and packing of **HL**[20] along the *c* axis. (c) Neighbouring group distances of TPE moieties from the *b* axis. (d) Slippage angles. Close proximity between (e) adjacent N and (f) separated neighboring salicylaldehyde groups in **HL**[20]; reproduced from ref. 190 with permission from Elsevier, Copyright 2024.

stacking interactions,[193] with a π···π distance of 4.507 Å and a significant slippage angle of 42.87 (Fig. 24(d)).

Salicylaldimine groups were found to be regionally packed, despite the close proximity of 3.475 Å between neighboring nitrogen atoms (Fig. 24(e)). Furthermore, the bulkiness of the methoxyphenyl group would have hindered the isomerization between salicylaldehyde amine groups (Fig. 24(f)) due to the lack of space between neighboring groups with the same conformation (Fig. 24(f)). It is possible that this conformational restriction may have hampered *cis–trans* isomerisation of the *cis*-keto form in the solid state and contributed to **HL^{20}**'s AIE fluorescence.[194] The degree of difficulty of the isomerization reaction can be ascertained by plotting potential energy curves using various molecular conformations. The DFT calculation shows that the energy difference between the enol and keto forms was 0.94 eV. Fig. 25(a) indicates that the enol form is more stable than the keto form. The twisted form of the *cis* keto conformation that comes from 60 (rotation of salicylaldehyde benzene is unstable because of large energy barriers) (clockwise (E = 0.73 eV) and anticlockwise (E = 0.90 eV)) following heating; this *trans* keto is missing and the colour quickly returns. By examining frontier orbital energies, Fig. 25(b) illustrates how the isomer's fluorescence changes. As the energy gap narrows, a thermally induced red shift occurs. Fig. 25(c) and (d) provide insights into the molecular motion of ground and excited states of the isomer using TD-DFT. Transformation of enol to *cis* keto form through the ESIPT process results in the occurrence of a red shift.[190]

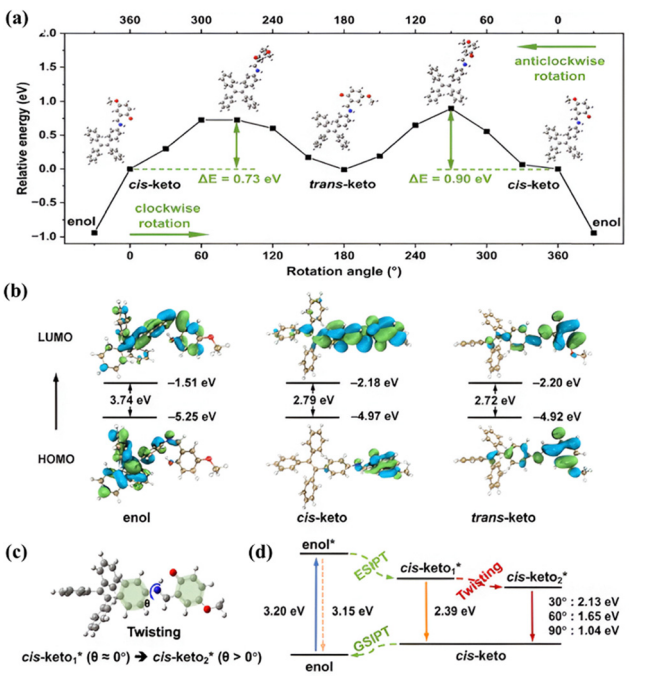

Fig. 25 (a) DFT-calculated relative energies for **HL^{20}** in the absence of solvent with different conformations from the enol to *cis*-keto to *trans*-keto forms. (b) Frontier molecular orbits and HOMO and LUMO energies of **HL^{20}** isomers, (c) twisted structure in the *cis*-keto*form, (d) schematic representation of the inactivation of **HL^{20}** with the keto–enol form *via* ESIPT, twisting and GSIPT; reproduced from ref. 190 with permission from Elsevier, Copyright 2024.

4.5 Intramolecular charge transfer ICT transition

Tetraphenylethene-based Schiff base ligand exhibited both an AIE behaviour and a hallmark of conventional ICT. Due to the prevention of C=N isomerisation in ligands, the boron complex (**HL^{5}**) produced bright AIE phenomena, red-shifted and increased emission, and reversible high contrast mechanofluorochromic behaviour. The synthesized **HL^{5}** sample exhibited a significant spectrum shift from 498 to 595 nm, as well as an emission colour change from brilliant green to orange upon grinding.[73] Molecular conformation and stacking mode data must be gathered to investigate the multi-stimulated response pathway further. By gradual crystallisation from a THF solution at room temperature, three environmentally responsive chromotropic molecules were produced as single crystals. According to the crystal data, **HL^{13}-H** is monoclinic with a space group of $P21/c$, while **HL^{13}-Cl** is a member of the triclinic system with a space group of $P\bar{1}$. Whereas **HL^{13}-Cl** has two molecules arranged in antiparallel π–π stacking within each unit cell, **HL^{13}-H** contains four molecules per unit cell, generating a quadrature structure.[55]

In the solid state, intermolecular hydrogen bonding (1.870 Å for **HL^{13}-H** and 1.862 Å for **HL^{13}-Cl**) improves stability (Fig. 26). **HL^{13}-Cl** exhibits a J-aggregate stacking mode with an interplane distance of 3.324–3.364 Å, whereas **HL^{13}-H** forms a 2D network structure that is expanded by intermolecular contacts. **HL^{13}-Br** is stacked and arranged similarly to **HL^{13}-Cl**. Fluorescence properties are influenced by several factors such as hydrogen bonds, stacking modes, and intermolecular interactions.[189–191]

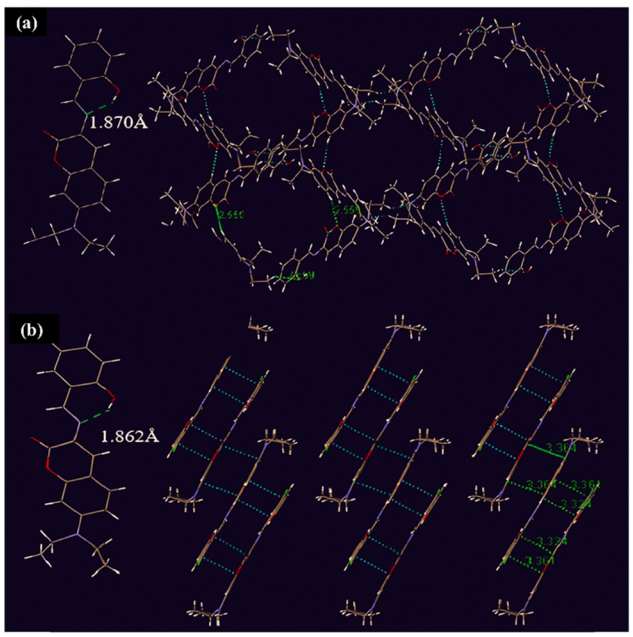

Fig. 26 Representation of structures of crystals and the molecular stackings of **HL^{13}-H** (A) and **HL^{13}-Cl** (B); reproduced from ref. 55 with permission from Elsevier, Copyright 2023.

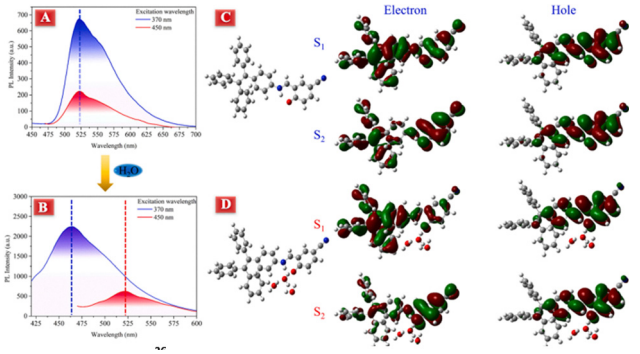

Fig. 27 PL spectra of the L^{26} compound in THF (A) and 10% water fraction with THF after 12 h standing (B). (C) and (D) Optimized keto structure of L^{26} and pertinent calculated orbitals of the solvated keto structure for the S1 and S2 state; reproduced from ref. 121 with permission from Elsevier, Copyright 2021.

Rigid intermolecular rotation limits luminescence in the single crystal structures of HL^{13}-**R**, causing aggregation-induced emission and mechanochromic characteristics.[55]

The use of electron–hole analysis and Kasha and anti-Kasha's rule to discuss L^{26} fluorescence behaviour has been reported by Sun *et al.* In essence, complex molecules in the condensed phase are the subject of Kasha's rule, which deals with photophysics. No matter which electronic state of equal multiplicity is excited, if each molecule absorbs one photon under photostationary conditions, the corresponding emission from the first excited electronic level is guaranteed by the fast internal conversion and vibrational relaxation.[195] The effects of anti-Kasha offer a crucial component that clarifies the mechanics underlying excited-state changes.[196] Fig. 27(A) and (B) clearly show the L^{26} fluorescence behaviour in water, which interacts with the water to cause a red shift. Intermolecular H-bonds between L^{26} and water molecules will progressively form upon the addition of water. Electron–hole analysis further revealed that, whilst the electron of the S_1 state is largely localised in the TPE molecule (Fig. 26(D)), the electron of the S_2 state of the solvated keto structure exhibited a significant distribution in the 2-hydroxy-5-cyanobenzaldehyde fragment.[197] Furthermore, the internal conversion rate between S_2 and S_1 of the solvated ketone structure will be significantly reduced due to the wide energy gap (0.54 eV) between S_2 and S_1.[198,199] These experimental and computational results confirmed the anti-Kasha property of solvated L^{26}. Nonetheless, the emission properties of L^{26} in THF corresponded with Kasha's rule, as demonstrated by fluorescence spectrum data and theoretical calculations (Fig. 27(A) and (C)).[121] Under the influence of water, Kasha's rule emission of this molecule clasps into a typical anti-Kasha's rule emission, which should essentially explain the fluorescence switch's distinctive dynamic stimuli-responsiveness.

5. Biomedical, environmental and industrial applications

In the above discussion, multi–stimuli responsiveness is shown in Schiff base-based monomers, polymers, and complexes. Due to these behaviour, a wide variety of applications are possible. The hydrophobic monomer (QHPMA, MAA) and a small amount of PEGDA as a chemical crosslinking agent were used to synthesize a hydrogel by free radical polymerization. The maximum tensile fracture stress reached 1.39 MPa, with a maximum tensile fracture strain of 162% and toughness up to 1.21 MJ m^{-3}. Additionally, the mechanical properties of the hydrogel can be regulated and enhanced by Zn^{2+} ions. The **P20** hydrogel exhibited highly selective fluorescence properties for Zn^{2+}. At a Zn^{2+} concentration of 0.1 M, the fluorescence intensity increased to 1851% of its value before complexation, and this intensity could be regulated by varying the Zn^{2+} concentration. The introduction of the hydrophobic monomer (*Z*)-*N*-(4-(2-(quinoline-2-methylene)hydrazine-1-carbonyl) phenyl)methyl acrylamide (QHPMA) has provided the hydrogel with anti-swelling properties and enhanced mechanical stability in water. Additionally, the incorporation of Schiff base–Zn^{2+} ion coordination endowed the hydrogel with strong antibacterial properties. Building on these improved properties, the **P20** hydrogel was developed and tested for underwater storage, dual shape memory functions, fluorescence encryption writing, and fluorescent solvent response. This high-strength, anti-swelling, and tough, fluorescent hydrogel shows potential for applications in underwater sensors, shape memory materials, solvent detection, and other related fields. Fig. 28 demonstrates this phenomenon very well.[53]

Schiff base chelates have also enabled temperature monitoring and imaging by leveraging their phosphorescence decay times. Optical oxygen sensing requires a longer decay time and high phosphorescence brightness. Due to the high optical transparency and good oxygen permeability, dye immobilized on polystyrene has shown immense potential in this area. In addition, it exhibits good mechanical properties, chemical robustness, and photophysical properties comparable to those of the solution. The immobilization of the dye causes a reduction in the decay time and luminescence quantum yield (F = 0.38 and t = 7.3 ms at room temperature and under anoxic conditions) since some of it may

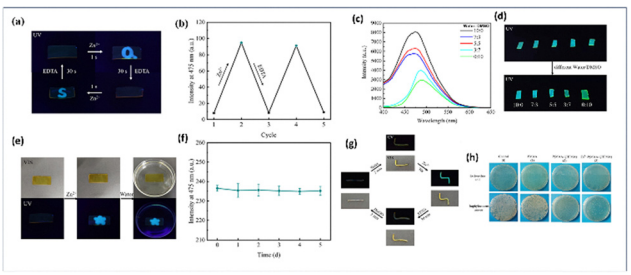

Fig. 28 Various applications of **P20**; (a) fluorescence encryption writing and erasure process; (b) intensity of hydrogel soaked between Zn^{2+} and EDTA solution; (c) fluorescence emission spectra; (d) optical images after soaking in mixed solvents with different ratios of water and DMSO; (e) underwater fluorescence information storage process in visible and UV light; (f) study of the fluorescence curve of the hydrogel after soaking in water for 5 days; (g) shape memory function; (h) bacteria plate figure for *Escherichia coli* and *Staphylococcus aureus* for detecting antibacterial activity; reproduced from ref. 53 with permission from Elsevier, Copyright 2022.

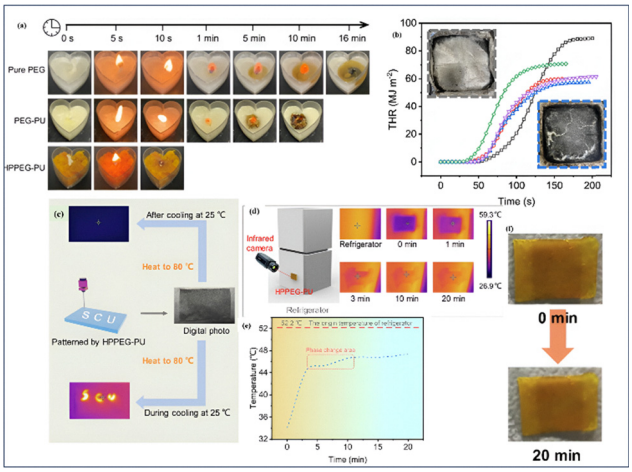

Fig. 29 (a) Fire-resistance performance by candle test of pure PEG, PEG4000-PU, and **P1**-4000; (b) total heat release rate curve; (c) imaging of thermosensitivity of **P1**-6000 in nonwoven fabric during heating or cooling; (d) infrared images (e), time–temperature curves, and shape stability (f) of **P1**-6000 on the refrigerator; reproduced from ref. 52 with permission from Elsevier, Copyright 2022.

aggregate in the polymer.[200] Polymeric phase change materials (PCMs) have attracted significant attention due to their no-leakage properties and significant latent heat capacity, making them valuable for thermal management. However, their flammability, limited recyclability, and low energy storage density have posed long-term challenges, restricting their applications in sustainable energy solutions. Linear polymeric solid–solid-PCM **P1** offers easy fire safety, recyclability, and high heat transition capacity by incorporating an aromatic Schiff base structure into its hard segment. Although **P1**-4000 has a low LOI value of 21%, it demonstrates good fire-resistance performance in the candle test (Fig. 29(a)). The potential of **P1** for thermosensitive imaging is due to its efficient thermal energy storage and release (Fig. 29(b)). Using **P1**-6000, patterned letters were created on nonwoven fabric and were tested by heating and cooling (Fig. 29(c)). The phase change in HPPEG6000-PU caused the patterned areas to exhibit higher temperatures and brighter patterns in thermal images. The stability of the patterned letters (SCU), even after temperature changes, demonstrates **P1**-6000 suitability for thermosensitive imaging applications (Fig. 29(d)). This phase change material (PCM), can help manage thermal peaks in electronic components due to its shape stability (Fig. 29(f)) and high thermal energy storage capacity. When applied to the surface of a refrigerator's heating device, **P1**-6000 maintained a stable temperature of about 46 °C, which is significantly lower than the original 52.2 °C (Fig. 29(e)). This stability is attributed to the solid–solid phase transition of P1-6000, making it an effective solution for managing overheating and storing excess heat in electronic devices.[52] **HL**^{20}'s fast and reversible thermochromic activity has made it an attractive candidate for thermochromic textiles, warning labels, thermal printing, as well as reversible patterning displays. Thermally and chemically stable Al_2O_3 is physically blended with HL20 and evenly dispersed onto the mold before being scraped to obtain the desired pattern. The fabricated fish pattern using **HL**^{20}/Al_2O_3 (1 : 2, v/v) displayed almost the same colour during 5 heating and cooling cycles. A warning label or temperature-sensitive sticker can serve as a warning indicator of high temperatures (Fig. 30). Similarly, mixing **HL**^{20} with white ink paste at various proportions is used in thermal printing, such as stamp printing, as shown in Fig. 30(e), with a good reversible colour shift. As expected, the composite material's PL spectra (Fig. 30(f)) peaked at 580 nm; compared to **HL**^{20}, the combined ink paste exhibited higher fluorescence intensity at temperatures ranging from 25 °C to 85 °C. This can be explained by **HL**^{20}'s restricted intramolecular mobility in the viscous environment of the ink.[190] A novel optical display device was developed to leverage the irreversible photochromic and reversible thermochromic properties of a chiral salicylaldehyde Schiff-derived molecule $\mathbf{H_2L}^{22}$. Blue text on a yellow background was created by sandwiching the sample between transparent and black glass layers and exposing it to UV light through a "USTB" mask, thanks to the photochromism of NACN-doped liquid crystals (LCs). As the temperature increased from 20 °C to 60 °C, the colour changed to red and the irradiated LCs became more isotropic, making the letters stand out on a black background. When temperatures exceeded 65 °C, the liquid crystals lost order, causing the text to vanish. During cooling, pressing the device switched the LC state, bringing the hidden message to life. At intermediate temperatures, text selectively appeared in non-irradiated zones, shifting hues with the cooling process. This innovative approach allows the device to record and reveal information through light and heat, offering a promising solution for privacy display technologies.[33] By connecting the amino groups of carboxymethyl chitosan (CMCS) with the aldehyde groups of oxidised hyaluronic acid (OHA) *via* a Schiff base reaction, a multifunctional hydrogel was created. This adaptable hydrogel **P7** is suitable for 3D printing, where the print head is combined with two precursor solutions (CMCS and OHA) before printing. For example, Fig. 30(g) illustrates the effective

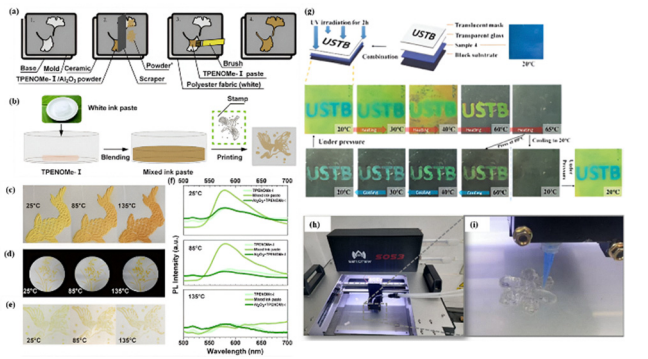

Fig. 30 (a) Schematic presentation of the patterning process using a mask with **HL**^{20}/Al_2O_3 powder (1: model; 2: scraping pattern with **HL**^{20}; 3: brushing pattern with **HL**^{20} colour paste; 4: obtained pattern); (b) pattern printing using **HL**^{20} and white ink paste using images of (c) fish, (d) orchid, and (e) bird patterns; (f) corresponding temperature-dependent PL spectra of **HL**^{20} composites; reproduced from ref. 190 with permission from Elsevier, Copyright 2024; (g) optical information recording and thermal-driving memory display process for $\mathbf{H_2L}^{22}$; reproduced from ref. 34 with permission from RSC, Copyright 2020; (h) and (i) 3D printing of hydrogel **P6**; reproduced from ref. 201 with permission from Elsevier, Copyright 2023.

Table 1 Schiff base organic crystals, metal complexes, and polymeric systems exhibing stimuli-responsive behaviour and various applications

S. no.	Responsive behaviour	Material types	Schiff-based material	Starting material	Characteristic properties	Applications	Ref.
1	Mechanochromism, luminescence	Schiff base organic crystal	**HL**[1]	4-(Diphenylamino)benzaldehyde, 3-hydroxy-2-naphthohydrazide	Twisted conformation and weak intermolecular interactions (C–H···π, π···π, and hydrogen bonds)	Smart devices	61
2	Mechanochromic luminescence	Schiff base organic crystal	**H_4L^2**	2-Hydroxy-1-naphthaldehyde, N^2,N^6-bis(2-aminophenyl)pyridine-2,6-dicarboxamide	Solvent molecule-dependent acidochromism	Ability to act as a sensitive chemosensor for Cu^{2+} ions	57
3	Mechanochromic and acidochromic	Schiff base zinc complex	**ML**[3]	3-(2-Benzothiazolyl)-2-hydroxybenzaldehyde, an aromatic amine (R-NH_2) and Zn(II)	Smaller dihedral angle and strong intermolecular interactions provide red shifted emission	Smart fluorescent materials	70
4	Mechanofluorochromic	Schiff base fluoroborate complex	**HL**[4]	3,5-Di-*tert*-butyl-2-hydroxybenzaldehyde, 4-(1,2,2-triphenylvinyl)aniline	Combination of locally excited state (LE), intramolecular charge-transfer (ICT), ESIPT and AIE mechanism	CO_3^{2-} and Zn^{2+} detection and reversible mechanofluorochromism	56
5	Mechanofluorochromic	Schiff base fluoroborate complex	**HL**[5]	Tetraphenyl ethene, $BF_3{\cdot}Et_2O$, 2-hydroxy-1-naphthaldehyde	Intramolecular charge transfer, aggregation-induced emission	—	73
6	Mechanochromic	Schiff base Zn complex	**H_2L^6**	Salicylhydrazide, zinc nitrate and (*E*)-2-hydroxy-*N*′-(quinolin-2-ylmethylene)benzohydrazide	C–H···π and hydrogen bond interaction	Good luminescence behaviour	74
7	Mechano optical	Schiff base zinc complex	**ML**[7]	4-(Diphenylamino)benzaldehyde, 3-aminopyridin-2(1*H*)-one	Phase transition from the crystalline to the amorphous state	Detection and information storage	62
8	Mechanochromic-photochromic	Schiff base zinc complex	**H_2L^{11}**	Nicotinic hydrazide and 5-bromosalicylaldehyde	Configuration changing process, ESIPT process, intramolecular hydrogen bonds	Chemosensor	127
9	Vapochromic and vapoluminescence	Schiff base zinc complex	**ML**[12]	2-Hydroxy-4-(undec10-enyloxy)benzaldehyde, 2,3-diaminomaleonitrile	Aggregation induced emission	Detection of *n*-butyl vapour	131
10	Optical and temperature	Schiff base metal complexes	**ML**[14]	4,5-Diaminophthalonitrile, 4-(dibutylamino)-2-hydroxybenzaldehyde	Luminescent	Optical oxygen sensing, optical temperature sensing and imaging	200
11	Thermochromic	Schiff base zinc complexes	**ML**[15], **ML**[16]	Chloro(trimethyl)silane, $Zn(OAc)_2{\cdot}2H_2O$, 3-(bis(2-ethylhexyl)amino)phenol, and 4-(3,6-di-*tert*-butyl-9*H*-carbazol-9-yl)-2-methoxybenzaldehyde, biaxially oriented polyethylene terephthalate (PET)	Long luminescence decay times oxygen-scavenging capabilities	Sensor for long-term temperature monitoring	205
12	Hydrostatic pressure		**P3**	TPE and rhodamine-B	Shearing and hydrostatic pressure luminescent	Fluorescent switch with multicoloured changes	65
13	Thermochromic	Schiff base organic crystals	**H_4L^{17}**, **H_4L^{18}**	3,3′-(4-Nitro-1,2-phenylene)bis(diazene-2,1-diyl)bis(2-hydroxy-5-nitrobenzaldeyde), 2-hydroxy aniline, 2-amino-4 nitrophenol	Thermochromism behaviour due to change in π-electron configuration induced by IPT in the ground state,	Multi–stimuli	79
14	Thermochromic	Schiff base polymer	**P1**	Methylene diphenyl diisocyanate, *p*-hydroxybenzaldehyde, *p*-phenyl enediamine, *N*,*N*-dimethylformamide	Thermal property and shape stability	Fire safety, thermo-sensitive imaging and thermal management	52
15	Thermochromic	Schiff base@MOF with polymer matrix	**H_2L^{23}**@MOF-808/PP-25	4-((2-Hydroxybenzylidene)amino) benzene sulfonic acid (HBABSA), MOF-808, polyvinyl alcohol (PVA) and poly(2-acrylamide 2-methyl-1-propane sulfonic acid) (PAMPS) as polymer matrixes	ESIPT mechanism	Remote control, thermal sensing, intelligent batteries	34
16	Thermochromic	Schiff base organic crystal	**HL**[20]	4-(1,2,2-Triphenylvinyl)aniline 4-methoxy-2-vinylphenol	ESIPT inspired AIE properties, polymorphism	Warning labels, thermochromic textiles, and thermal printing	190
17	Thermochromic	Schiff base organic crystal	**H_2L^{21}**	2,2′-Bis(trifluoromethyl)benzidine, salicylaldehyde	Enol–keto isomerization, AIE properties, aggregated state, and excited state intramolecular proton transfer (ESIPT) process involved	—	80

Table 1 (*continued*)

S. no.	Responsive behaviour	Material types	Schiff-based material	Starting material	Characteristic properties	Applications	Ref.
18	Mechano, thermo, pH	Schiff base organic crystal	**HL**[13]	3-Amino-7-diethylamino coumarin, Salicylaldehyde	AIE, hydrogen bonds, intermolecular interactions	Multilevel anti-counterfeiting labels	55
19	Thermo-pH	Schiff base polymer	**P2**	*N*-Isopropyl acrylamide, DMAMVA, and styrene	Polymer chain's hydrophilic/hydrophobic groups strongly affect the contact angles in water and pH of solutions	Separation technology of biomolecules	129
20	Thermo-Opto	Schiff base organic crystal	H_2L[22]	2,4-Dihydroxybenzaldehyde, 2-ethylhexyl bromide, 1,1′-bi-2-naphthol, *p*-nitrobenzoic acid	Intramolecular hydrogen transfer from an enol structure to a *cis*-keto structure in NaCN	Responsive materials for privacy information displays	33
21	Thermo and stress	Schiff base polymer	Dendritic OEG unit with Schiff base	OEG based dendritic macromonomer and aminoethyl methacrylate	Dendritic OEG units and imine bond for thermal, pH and stress responsive and tunability	Self-healing	206
22	Thermal and vapor	Schiff base Zn complex	**ML**[19]	5-*t*-Butyl-2-hydroxybenzaldehyde, 2,3-diaminomaleonitrile-	Mechanochromic and acidochromic properties	Chemosensors (vapochromic detection of volatile organic compounds)	130
23	Mechanochromism, thermochromism, protonation effect	Schiff base organic crystal	**HL**[10]	4-Diethylamino-2-hydroxybenzaldehyde, ethyl nitroacetate, piperidine	ESIPT and AIE mechanism	Discriminating $CHCl_3$ from organic solvents assisted by UV irradiation	185
24	Stress–Strain	Schiff base polymer	**P4**	Poly(ethylene glycol) methacrylate (PEGMA), 4-carboxybenzaldehyde, benzylideneaniline, *N*-(4-methylbenzy-lidene)-3-chloroaniline and methylene diphenyl diisocyanate (MDI), and 4,4′-diaminodiphenyl methane (DDM)	Bond flexibility	Smart material self-healing and remolding	207
25	Stress–strain	Schiff base polymer	**P5**	Dialdehyde-modified hyaluronic acid (HA), cystamine	Bond flexibility, dynamic covalent bonds	Drug delivery, bioprinting, smart robots and tissue regeneration	103
26	Stress–strain and thermal	Schiff base polymer	**P8**	Indole-3-carboxaldehyde, 4-aminobenzohydrazide, methacryloyl chloride, MAA, PEGA, triethylamine	Synergistic effect of hydrophobic association of IHPMA and multiple hydrogen bonds of PEGA, P(MAAPEGA-IHPMA) hydrogel, excellent mechanical properties, fluorescence properties with Zn^{2+}	Temperature control materials, anti-fatigue materials and flexible sensors	36
27	Stress–strain	Schiff base polymer	Combination of RAFT polymerization and the formation of Schiff base bond	VMA, ethyl cellulose macroinitiator and LA	coordination between dynamic imine bonds and polymer chain movement capability	Adhesive strength and self-healing ability	208
28	Stress–strain	Schiff base polymer	**P6**	CMCS and OHA	Dynamic bond	3D printing	201
29	Stress–strain	Schiff base polymer	**P7**	Poly(vinyl alcohol) PVA, 4-formylbenzoic acid, 3,4-diaminobenzoic acid (3,4-DABA) and 4-(dimethylamino) pyridine	Bond flexibility	Self-healing ability and mechanical properties for biomedical applications	102
30	Piezochromic	Schiff base organic crystal	**HL**[9]	3-Amino acetophenone, 2-hydroxy-1-naphthaldehyde	π–π stacking, AIE emission	Pressure sensing, data storage, security technologies	25
31	Solvent	Schiff base organic crystal	**L**[26]	4-Tetraphenylethenyl amine, 3-formylbenzonitrile	Aggregation-induced emission enhancement (AIEE) property	Data security, data protection, fluorescence detection	121
32	Solvent	Schiff base organic crystal	**L**[27]	2-Hydrazinyl-4.6-dimethylpyrimidine, pyrene-1-carbaldehyde	Solvatochromic behaviour due to the polarity of medium and hydrogen bonding properties	Potential sensor for quantitative detection of Hg^{2+} in different samples	122
33	Solvent		**L**[28]	9-Anthracenecarboxaldehyde and aromatic amine	Solute–solvent interaction with relative polarities in ground and excited state	Fe^{3+} sensing	117

Table 1 (*continued*)

S. no.	Responsive behaviour	Material types	Schiff-based material	Starting material	Characteristic properties	Applications	Ref.
		Schiff base organic crystal					
34	Solvent	Schiff base polymer	**P20**	4-Aminobenzohydrazide, 2-quinolinecarboxaldehyde, methacryloylchloride, methacrylic acid, diacrylate, zinc acetate dihydrate	High-strength, tough, and anti-swelling fluorescent hydrogel	Underwater sensors, solvent detection, shape memory materials	53
35	Solvent	Schiff base organic crystal	**L**[29], **L**[30]	2-Amino-4-methylben zothiazole and 2-amino-6-chlorobenzothiazole	Different polarity with solvents	Metal ion detection	123
36	Solvent	Schiff base organic crystal	**HL**[31]	3-Ethoxy-2-hydroxybenzaldehyde, 4-aminotoluene	ESIPT mechanism	Optoelectronic device technology, chemosensing, biological or clinical applications, and solar cell designs	124
37	Solvent	Schiff base polymer	**P19**	(*E*)-5-(4-(Dimethylamino)styryl)thieno[3,2-*b*]thiophene-2-carbaldehyde, protein chain	Π-bridge formation, ICT	Covalent probes and sensors to analyze the protein misfolding and aggregation	202
38	Solvent	Schiff base organic crystal	**L**[32]	5-Aminoquinoline, 2,5-dibromothiophene-3-carboxaldehyde	π–π^* transition, ICT, H-bonding	Diverse applications of Schiff bases in AIEE and analyte detection	125

printing of a petal-shaped hydrogel using a 6% solution of both OHA and CMCS. The application potential of intelligent hydrogels is greatly increased when they are combined with 3D printing. Research on the mechanical strength of 3D-printed hydrogels demonstrates that they are comparable to that of traditionally manufactured hydrogels, as seen in Fig. 30(g) and (h). Furthermore, by modifying the precursor concentration during the printing process, these hydrogel's mechanical properties can be adjusted to meet various functional needs. The integration of state-of-the-art hydrogel materials with 3D printing technology opens up possibilities for new and flexible applications.[201] Shen *et al.* showed that aldehyde-containing probes can effectively modify lysine residues in aggregated proteins. The results of spectral analysis, mass spectrometry, and electrophoresis demonstrated that Schiff base production was primarily observed in aggregated proteins rather than folded ones. This recently found chemical response held for many protein types and probe derivatives. The solvatochromism of the probe following Schiff base formation in living cells revealed variations in the local polarity and morphology of the aggregated proteome. This work paves the way for exploring other covalent reactions to design probes and sensors for analyzing protein misfolding and aggregation processes.[202] Apart from these applications, Zn(II) complexes, specially Schiff base complexes, due to their promising luminescent properties, have also been utilized for the generation of ZnO nanoparticles *via* thermal decomposition of the complex for their further exploitation for various biomedical applications due to their fluorescence properties.[203]

Here, Table 1 summarizes all the Schiff base crystals, complexes, and their polymers along with their precursors, stimuli behaviour, and applications.

6. Future perspective and challenges

This review highlights the substantial advances in the development of various stimuli-responsive materials through Schiff base chemistry. Due to their unique structural and chemical properties, Schiff base ligands can easily conjugate with metal ions and diverse polymeric systems. This flexibility enables the creation of materials with a wide range of properties, including improved conjugation, mechanical strength, stretchability, and switchable behaviour in electron transfer processes, making them great candidates for smart, responsive systems. One of the key advantages of Schiff base reactions is their simplicity in chemical synthesis. Furthermore, when the C═N bond is conjugated with an aromatic system, it can form an extended conjugate structure with distinct features from a single aromatic unit. For instance, Schiff base linkages with compounds like coumarin, TPA, TPE, pyridine, and other heterocyclic or polymeric systems—including LA, PEG, PVA, hyaluronic acid, VMA, amino acids, protein chain, carboxymethyl chitosan, and aminoethyl methacrylate—offer tremendous potential for multi–stimuli responsive behaviour. Applications such as sensing, self-healing, adhesiveness, 3D printing, drug delivery, temperature control, antifatigue materials, and robotics could be possible only due to enhanced stimuli-responsive behaviour or using this

chemistry. Schiff bases derived from salicylaldehyde, naphthaldehyde, and their substituted variants exhibit promising applications in areas such as chemical sensors, pressure sensors, and anticounterfeiting technologies, leveraging mechanochromic, thermochromic, piezochromic, and acidochromic properties. In 2023, Zhu *et al.* utilized the dynamic characteristics of imine formation to introduce a solvent-responsive approach for the intelligent transition between an amorphous ionic polyimine membrane and a crystalline organic molecular cage. Remarkably, this transformation occurs without the need for additional building blocks, as the aldehyde and amine components self-correct in response to the solvent environment, adapting to form either a polymer network or a molecular cage.[204] This phenomenon illustrates the capacity of imine chemistry to facilitate the development of intelligent, adaptive materials that respond to environmental stimuli. Despite their developments and practical applications, Schiff base-based multi–stimuli materials confront several substantial obstacles. One major concern is the difficulty of synthesizing these materials with the necessary characteristics due to the instability of Schiff base couplings, which might degrade with time. The need for exact design, especially in hydrogels, complicates synthesis and can result in poor mechanical stability and restricted strength. Furthermore, environmental sensitivity, such as interference in pH-responsive materials in complex environments, hampers their operation.[204–206] Although Schiff base-based multi–stimuli materials have enormous potential for a wide range of applications, various challenges must be addressed before they can be completely realized.[209–211] These challenges include complex synthesis processes, optimizing mechanical properties, sensitivity to environmental factors, scaling up production, and the need for advanced tools and techniques for characterization. Addressing these challenges will require interdisciplinary collaboration among chemists, materials scientists, and engineers to develop innovative solutions that enhance the functionality and practical applicability of Schiff base-based materials in real-world scenarios.

Author contributions

Dimpi Gupta, Divyanshu Singh, and Anushka Koranne: original writing, conceptualization, and data analysis; Chandni Singh: Data analysis; Ashish Kumar Singh, Sunil Kumar Singh, and Rajat Pratap Singh: manuscript checking, and supervision.

Conflicts of interest

The authors declare that they have no known competing financial or personal relationships that could have appeared to influence the work reported in this paper.

Abbreviations

TICT	Twisted intramolecular charge transfer
AIE	Aggregation-induced emission
TPE	Tetraphenylethene
THF	Tetrahydrofuran
DFT	Density functional theory
LE	Locally excited
PEG	Polyethylene glycol
MAA	Methacrylic acid
THF	Tetrahydrofuran
HLCT	Hybridized local and charge transfer
AIEE	Aggregation-induced enhanced emission
TFA	Trifluoroacetic acid
TEA	Triethylamine
PEG	Polyethylene glycol
CMCS	Carboxymethyl chitosan
OHA	Oxidized hyaluronic acid
MSH	Metallo-supramolecular hydrogels
PU	Polyurethane
ICT	Intramolecular charge transfer
PXRD	Powder X-ray diffraction
DCM	Dichloromethane
MFC	Mechanofluorochromic
HOMO	Highest occupied molecular orbital
FESEM	Field emission scanning electron microscopy
VMA	Vanillin methacrylate
LA	Lauryl methacrylate
DMAMVA	2-((Dimethylamino)methyl)-4-formyl-6-methoxyphenyl acrylate
HBI	2-(2′-Hydroxyphenyl)benzimidazoles
Sas	Salicylideneanilines
HBABSA	4-((2-Hydroxybenzylidene)amino)benzenesulfonic acid
RAFT	Reversible addition–fragmentation chain transfer
IHPMA	(*Z*)-*N*-(4-(2-((1*H*-Indol-3-yl)methylene)hydrazino-1-carbonyl)phenyl)methacrylamide
OEG	Oligoethylene glycol
PET	Polyethylene terephthalate
Pt-TFPP	Platinum(II) *meso*-(pentafluoro phenyl)porphyrin
PEGMA	Poly(ethylene glycol) methacrylate
PAMPS	Poly(2-acrylamide 2-methyl-1-propane sulfonic acid)
MDI	Methylene diphenyl diisocyanate
DDM	4,4′-Diaminodiphenyl methane
HA	Hyaluronic acid
3,4-DABA	3,4-Diaminobenzoic acid
TPA	Triphenylamine
QHPMA	(*Z*)-*N*-(4-(2-(quinoline-2-methylene)hydrazine-1-carbonyl) phenyl) methyl acrylamide
PEGDA	Polyethylene glycol diacrylate

Data availability

No primary research results, software or code have been included and no new data were generated or analysed as part of this review.

Supplementary information is available. See DOI: **https://doi.org/10.1039/d5ma00109a**.

Acknowledgements

The authors acknowledge the contributions of scientists studying in this area, who assisted them in various ways while they wrote this review. Dimpi Gupta and Anushka Koranne thanks the UGC for the university fellowship. Divyanshu Singh thanks the SJSGC Fellowship (202223-UGCES-22-GE-UTT-F-SJSGC-3353) provided by UGC.

References

1 J. W. Dunlop, R. Weinkamer and P. Fratzl, *Mater. Today*, 2011, **14**, 70–78.
2 M. E. McConney, K. D. Anderson, L. L. Brott, R. R. Naik and V. V. Tsukruk, *Adv. Funct. Mater.*, 2009, **19**, 2527–2544.
3 Y. Bar-Cohen, *Biomimetics: Biologically Inspired Technology, in II Eccomas Thematic Conference on Smart Structures and Materials*, ed. C. M. Soares, CRC Press, Lisbon, Portugal, 2005, pp. 7–15.
4 M. J. Rodriguez, J. Brown, J. Giordano, S. J. Lin, F. G. Omenetto and D. L. Kaplan, *Biomaterials*, 2017, **117**, 105–115.
5 T. Dolui, T. S. Natarajan, J. Chanda, P. Ghosh, R. Mukhopadhyay, S. Wießner, G. Heinrich, A. Das and S. S. Banerjee, *Adv. Eng. Mater.*, 2023, **25**, 2300584.
6 Z. Wang, B. Zhang, Q. He, H. Chen, J. Wang, Y. Yao, N. Zhou and W. Cui, *Research*, 2023, **6**, 0122.
7 R. Geryak and V. V. Tsukruk, *Soft Matter*, 2014, **10**, 1246–1263.
8 I. Apsite, S. Salehi and L. Ionov, *Chem. Rev.*, 2021, **122**, 1349–1415.
9 B. Xia, A. Miriyev, C. Trujillo, N. Chen, M. Cartolano, S. Vartak and H. Lipson, *Actuators*, 2020, **9**, 62.
10 T. Mullin, S. Deschanel, K. Bertoldi and M. C. Boyce, *Phys. Rev. Lett.*, 2007, **99**, 084301.
11 J. Liu, Y. Gao, Y.-J. Lee and S. Yang, *Trends Chem.*, 2020, **2**, 107–122.
12 W. Tanaka, H. Shigemitsu, T. Fujisaku, R. Kubota, S. Minami, K. Urayama and I. Hamachi, *J. Appl. Chem. Sci.*, 2019, **141**, 4997–5004.
13 H. Okamoto, Y. Katagiri, M. Nakano and A. Usuki, *J. Appl. Polym. Sci.*, 2014, **131**, 41004.
14 M. Pannipara, A. G. Al-Sehemi, A. Kalam, A. M. Asiri and M. N. Arshad, *SAA*, 2017, **183**, 84–89.
15 S. Yang, X. Wang, Z. Hu and D. Guo, *Colloids Surf., A*, 2021, **615**, 126293.
16 Z.-Y. Yin, J.-H. Hu, K. Gui, Q.-Q. Fu, Y. Yao, F.-L. Zhou, L.-L. Ma and Z.-P. Zhang, *J. Photochem. Photobiol., A*, 2020, **396**, 112542.
17 J.-C. Qin, B.-d Wang, Z.-Y. Yang and K.-c Yu, *Sens. Actuators, B*, 2016, **224**, 892–898.
18 H. Zhao, X. Zhang, K. Chen, W. Wu, S. Li, T. Wang, X. Huang, N. Wang, L. Zhou and H. Hao, *CrystEngComm*, 2023, **25**, 2600–2606.
19 W. Wu, K. Chen, X. Zhang, T. Wang, S. Li, H. Zhao, L. Zhou, X. Huang and H. Hao, *Chem. – Eur. J.*, 2023, **29**, e202202598.
20 E. L. de Araújo, H. F. G. Barbosa, E. R. Dockal and É. T. G. Cavalheiro, *Int. J. Biol. Macromol.*, 2017, **95**, 168–176.
21 Y. Xin and J. Yuan, *Polym. Chem.*, 2012, **3**, 3045–3055.
22 S. A. Lee, G. R. You, Y. W. Choi, H. Y. Jo, A. R. Kim, I. Noh, S.-J. Kim, Y. Kim and C. Kim, *Dalton Trans.*, 2014, **43**, 6650–6659.
23 T. Mukherjee, J. C. Pessoa, A. Kumar and A. R. Sarkar, *Dalton Trans.*, 2013, **42**, 2594–2607.
24 D. P. Singh, R. Dwivedi, A. K. Singh, B. Koch, P. Singh and V. P. Singh, *Sens. Actuators, B*, 2017, **238**, 128–137.
25 P. Yadav, A. K. Singh, C. Upadhyay and V. P. Singh, *Dyes Pigm.*, 2019, **160**, 731–739.
26 P. Yadav, S. Gond, A. K. Singh and V. P. Singh, *J. Lumin.*, 2019, **215**, 116704.
27 R. Dwivedi, D. P. Singh, S. Singh, A. K. Singh, B. S. Chauhan, S. Srikrishna and V. P. Singh, *Org. Biomol. Chem.*, 2019, **17**, 7497–7506.
28 S. Liao, L. Tang and J. Qu, *Polym. Adv. Technol.*, 2021, **32**, 1844–1852.
29 R. Pandey, P. Kumar, A. K. Singh, M. Shahid, P.-Z. Li, S. K. Singh, Q. Xu, A. Misra and D. S. Pandey, *Inorg. Chem.*, 2011, **50**, 3189–3197.
30 S. D. Dwivedi, A. K. Singh, S. K. Singh, S. Sharma, M. Chandra and D. S. Pandey, *Eur. J. Inorg. Chem.*, 2008, 5666–5673.
31 C. Gautam, A. Singh, A. Singh, A. K. Singh, V. K. Sharma and P. Kumar, *J. Mol. Struct.*, 2021, **1243**, 130928.
32 D. P. Singh, C. Singh, S. K. Singh, R. Dwivedi, A. K. Singh and V. P. Singh, *Eur. J. Chem.*, 2022, **14**, 99–108.
33 L. Ren, W. He, M. Wei, S. Luo, D. Yao, Z. Yang, D. Wang and H. Cao, *J. Mater. Chem. C*, 2020, **8**, 561–566.
34 Z. Du, F. Zhang, H. Lin, W. Guo, M. Tian, K. Yu, D. Gao and F. Qu, *ACS Appl. Mater. Interfaces*, 2023, **15**, 10064–10074.
35 F. Zheng, J. Shi, S. Zhang, K. Liu and L. Xu, *ChemistrySelect*, 2023, **8**, e202301647.
36 W. Lu, J. He, H. Zhang and J. Qu, *Polym. Adv. Technol.*, 2023, **34**, 3370–3379.
37 L. Tang, J. Huang, H. Zhang, T. Yang, Z. Mo and J. Qu, *Eur. Polym. J.*, 2020, **140**, 110061.
38 L. Tang, S. Liao and J. Qu, *ACS Appl. Mater. Interfaces*, 2018, **10**, 27365–27373.
39 L. Tang, X. Chen, L. Wang and J. Qu, *Polym. Chem.*, 2017, **8**, 4680–4687.
40 C. Lu, C. Wang, J. Wang, Q. Yong and F. Chu, *J. Chem. Eng.*, 2021, **425**, 130652.
41 J. Schull, *J. Behav. Brain Sci.*, 1990, **13**, 63–75.
42 L. C. van Loon, *Trends Plant Sci.*, 2016, **21**, 286–294.
43 J. Böhm, S. Scherzer, E. Krol, I. Kreuzer, K. Von Meyer, C. Lorey, T. D. Mueller, L. Shabala, I. Monte and R. Solano, *Curr. Biol.*, 2016, **26**, 286–295.
44 C. Cadart, E. Zlotek-Zlotkiewicz, M. Le Berre, M. Piel and H. K. Matthews, *Dev. Cell*, 2014, **29**, 159–169.
45 A. C. Lloyd, *Cell*, 2013, **154**, 1194–1205.
46 D. A. Fletcher and R. D. Mullins, *Nature*, 2010, **463**, 485–492.
47 I. Ferain, C. A. Colinge and J.-P. Colinge, *Nature*, 2011, **479**, 310–316.

48 J. Hwang, M. Pototschnig, R. Lettow, G. Zumofen, A. Renn, S. Götzinger and V. Sandoghdar, *Nature*, 2009, **460**, 76–80.
49 Z. Shi, *Advanced artificial intelligence*, World Scientific, Singapore, 2019.
50 X. Zhang, L. Chen, K. H. Lim, S. Gonuguntla, K. W. Lim, D. Pranantyo, W. P. Yong, W. J. T. Yam, Z. Low and W. J. Teo, *Adv. Mater.*, 2019, **31**, 1804540.
51 J. Xu, Y. Liu and S.-H. Hsu, *Molecules*, 2019, **24**, 3005.
52 P.-P. Zhao, P. Lu, Z.-Y. Zhao, S.-W. Chen, X.-Y. Li, C. Deng and Y.-Z. Wang, *J. Chem. Eng.*, 2022, **437**, 135461.
53 H. Zhang, J. He and J. Qu, *Eur. Polym. J.*, 2022, **178**, 111487.
54 H. Goyal, V. Kumar, A. K. Saini, G. Kedawat, B. K. Gupta and R. Gupta, *Mater. Today Chem.*, 2023, **27**, 101306.
55 X. Wang, J. Shu, T. Ni, C. Xu, J. Tang, B. Xu, X. Liu, K. Zhang and W. Jiang, *Dyes Pigm.*, 2023, **208**, 110820.
56 J. Jia and H. Zhao, *Org. Electron.*, 2019, **73**, 55–61.
57 L. Shen, C.-J. Yu, H.-F. Xie, N. Xu, H. Xu, Y.-L. Huang, C. Redshaw, X. Feng and Q.-L. Zhang, *Mater. Chem. Front.*, 2022, **6**, 2491–2498.
58 T. Han, X. Gu, J. W. Lam, A. C. Leung, R. T. Kwok, T. Han, B. Tong, J. Shi, Y. Dong and B. Z. Tang, *J. Mater. Chem. C*, 2016, **4**, 10430–10434.
59 C. Duan, Y. Zhou, G.-G. Shan, Y. Chen, W. Zhao, D. Yuan, L. Zeng, X. Huang and G. Niu, *J. Mater. Chem. C*, 2019, **7**, 3471–3478.
60 X.-W. Chen, L.-H. He, P. Ju, J.-L. Chen, S.-J. Liu and H.-R. Wen, *J. Mater. Chem. C*, 2020, **8**, 16160–16167.
61 Q.-F. Liang, H.-W. Zheng, D.-D. Yang and X.-J. Zheng, *Cryst. Growth Des.*, 2022, **22**, 3924–3931.
62 Z.-G. Xia, Y.-S. Shi, T. Xiao and X.-J. Zheng, *CrystEngComm*, 2024, **26**, 1015–1021.
63 V. Gokul, D. Devadiga and T. Ahipa, *Dyes Pigm.*, 2021, **195**, 109692.
64 T. Seki, Y. Takamatsu and H. Ito, *J. Appl. Chem. Sci.*, 2016, **138**, 6252–6260.
65 X. Liu, C. Ma, A. Li, W. Xu, Z. Ma and X. Jia, *J. Mater. Chem. C*, 2019, **7**, 8398–8403.
66 S. S. Pasha, H. R. Yadav, A. R. Choudhury and I. R. Laskar, *J. Mater. Chem. C*, 2017, **5**, 9651–9658.
67 H.-W. Zheng, M. Wu, D.-D. Yang, Q.-F. Liang, J.-B. Li and X.-J. Zheng, *Inorg. Chem.*, 2021, **60**, 11609–11615.
68 S. Li, M. Wu, Y. Kang, H.-W. Zheng, X.-J. Zheng, D.-C. Fang and L.-P. Jin, *Inorg. Chem.*, 2019, **58**, 4626–4633.
69 H.-W. Zheng, S. Li, M. Wu, Y. Kang, J.-B. Li, Q.-F. Liang, X.-J. Zheng, D.-C. Fang and L.-P. Jin, *J. Mater. Chem. C*, 2020, **8**, 4246–4252.
70 H.-W. Zheng, D.-D. Yang, Q.-F. Liang and X.-J. Zheng, *Dalton Trans.*, 2021, **50**, 16803–16809.
71 Q. Li and Z. Li, *Acc. Chem. Res.*, 2020, **53**, 962–973.
72 Y. Gong, S. He, Y. Li, Z. Li, Q. Liao, Y. Gu, J. Wang, B. Zou, Q. Li and Z. Li, *Adv. Opt. Mater.*, 2020, **8**, 1902036.
73 T. Sun, D. Cheng, Y. Chai, J. Gong, M. Sun and F. Zhao, *Dyes Pigm.*, 2019, **170**, 107619.
74 Y.-B. Yan, R.-W. Yang, H.-W. Zhang, Y. Zhang and W.-K. Dong, *J. Mol. Struct.*, 2024, **1299**, 137148.
75 Y. Sagara, T. Mutai, I. Yoshikawa and K. Araki, *J. Appl. Chem. Sci.*, 2007, **129**, 1520–1521.
76 Q. Qi, J. Qian, X. Tan, J. Zhang, L. Wang, B. Xu, B. Zou and W. Tian, *Adv. Funct. Mater.*, 2015, **25**, 4005–4010.
77 M. Chen, W. Chen, Q. Zhu, L. Yang, X. Zhang, D. Xie, J. Chen, Y. Wu, Y. Zhu and M. Zhu, *J. Fluoresc.*, 2024, 1–12.
78 F. Han, R. Zhang, Z. Zhang, J. Su and Z. Ni, *RSC Adv.*, 2016, **6**, 68178–68184.
79 Ö. Özdemir, *J. Photochem. Photobiol., A*, 2019, **380**, 111868.
80 Z. Wu, J. Xu, Z. Wu, R. Zhao and L. Hou, *J. Photochem. Photobiol., A*, 2024, **453**, 115668.
81 A. Hakami, S. S. Srinivasan, P. K. Biswas, A. Krishnegowda, S. L. Wallen and E. K. Stefanakos, *J. Coat. Technol. Res.*, 2022, **19**, 377–402.
82 E. Leonard, C. Takeda and T. Akitsu, *Colorants*, 2024, **3**, 53–72.
83 Y. Wang, Z. Qiu, Z. Lang, Y. Xie, Z. Xiao, H. Wang, D. Liang, J. Li and K. Zhang, *Adv. Mater.*, 2021, **33**, 2005263.
84 H. Xu, L. Jiang, A. Yuan, Y. Lei, Z. Wei, Y. Wang and J. Lei, *J. Chem. Eng.*, 2021, **421**, 129833.
85 S. W. Choi, Y. Zhang and Y. Xia, *Angew. Chem., Int. Ed.*, 2010, **49**, 7904–7908.
86 J. Ma, T. Ma, J. Cheng and J. Zhang, *Energy Storage Mater.*, 2021, **39**, 294–304.
87 R. Zhang, C. Liu, C. Wei, J. Huang, X. Zou, Y. Feng, S. Ang, S. Guo, J. Qu, N. Qing, C. Tang, X. Zhou, M. Chen and L. Tang, *Adv. Mater. Technol.*, 2023, **8**, 2201527.
88 Y. Li, H. Li, W. Jin, X. Xu, H. Liu, Y. Ding, G. Wang, T. Zhang, Q. Peng and J. He, *Dyes Pigm.*, 2022, **202**, 110295.
89 C. Alkan, E. Günther, S. Hiebler, Ö. F. Ensari and D. Kahraman, *Sol. Energy*, 2012, **86**, 1761–1769.
90 T. Harlé, G. T. Nguyen, B. Ledesert, Y. Mélinge and R. L. Hebert, *Thermochim. Acta*, 2020, **685**, 178191.
91 K. Peng, C. Chen, W. Pan, W. Liu, Z. Wang and L. Zhu, *Sol. Energy Mater. Sol. Cells*, 2016, **145**, 238–247.
92 C. Chen, W. Liu, Z. Wang, K. Peng, W. Pan and Q. Xie, *Sol. Energy Mater. Sol. Cells*, 2015, **134**, 80–88.
93 Z. Cao, Y. Peng, T. Yan, S. Li, A. Li and G. A. Voth, *J. Appl. Chem. Sci.*, 2010, **132**, 11395–11397.
94 N. Agmon, *Chem. Phys. Lett.*, 1995, **244**, 456–462.
95 G. A. Luduena, T. D. Kühne and D. Sebastiani, *Chem. Mater.*, 2011, **23**, 1424–1429.
96 F. Li, X. Cai, G. Liu, H. Xu and W. Chen, *Adv. Funct. Mater.*, 2023, **33**, 2300701.
97 L. Shi, P. Ding, Y. Wang, Y. Zhang, D. Ossipov and J. Hilborn, *Macromol. Rapid Commun.*, 2019, **40**, 1800837.
98 T. C. Tseng, L. Tao, F. Y. Hsieh, Y. Wei, I. M. Chiu and S. H. Hsu, *Adv. Mater.*, 2015, **27**, 3518–3524.
99 S. Talebian, M. Mehrali, N. Taebnia, C. P. Pennisi, F. B. Kadumudi, J. Foroughi, M. Hasany, M. Nikkhah, M. Akbari and G. Orive, *Adv. Sci.*, 2019, **6**, 1801664.
100 W. Li, B. Wang, M. Zhang, Z. Wu, J. Wei, Y. Jiang, N. Sheng, Q. Liang, D. Zhang and S. Chen, *Cellulose*, 2020, **27**, 2637–2650.
101 A. Wolfel, C. I. A. Igarzabal and M. R. Romero, *Eur. Polym. J.*, 2020, **140**, 110038.
102 T. Takács, M. M. Abdelghafour, Ł. Lamch, I. Szenti, D. Sebők, L. Janovák and Á. Kukovecz, *Eur. Polym. J.*, 2022, **168**, 111086.

103 S. Li, M. Pei, T. Wan, H. Yang, S. Gu, Y. Tao, X. Liu, Y. Zhou, W. Xu and P. Xiao, *Carbohydr. Polym.*, 2020, **250**, 116922.
104 X. Yang, P. Zhao, J. Qu and R. Liu, *Luminescence*, 2015, **30**, 592–599.
105 O. Wichterle and D. Lim, *Nature*, 1960, **185**, 117–118.
106 Y. Li, J. Rodrigues and H. Tomás, *Chem. Soc. Rev.*, 2012, **41**, 2193–2221.
107 Y. Yang and M. W. Urban, *Chem. Soc. Rev.*, 2013, **42**, 7446–7467.
108 L. Tang, S. Liao and J. Qu, *ACS Appl. Mater. Interfaces*, 2019, **11**, 26346–26354.
109 Y.-L. Sang, X.-S. Lin and W.-D. Sun, *Acta Chim. Slov.*, 2020, **67**, 581–585.
110 L. Abdel-Rahman, A. Abu-Dief, F. Atlam, A. H. Abdel-Mawgoud, A. Alothman, A. Alsalme and A. Nafady, *J. Coord. Chem.*, 2020, **73**, 3150–3173.
111 E. V. Puttock, J. D. Fradgley, D. S. Yufit and J. G. Williams, *Dalton Trans.*, 2019, **48**, 15012–15028.
112 Y. Yuan, H. Zhang and J. Qu, *ACS Appl. Polym. Mater.*, 2021, **3**, 4512–4522.
113 J. He, Y. Yuan, L. Tang and J. Qu, *Polym. Adv. Technol.*, 2022, **33**, 1385–1393.
114 C. Liu, R. Zhang, P. Li, J. Qu, P. Chao, Z. Mo, T. Yang, N. Qing and L. Tang, *ACS Appl. Mater. Interfaces*, 2022, **14**, 26088–26098.
115 H. Zhang, J. He, T. Peng and J. Qu, *ACS Appl. Polym. Mater.*, 2022, **4**, 7575–7586.
116 K. Li, Y. Xiang, X. Wang, J. Li, R. Hu, A. Tong and B. Z. Tang, *J. Appl. Chem. Sci.*, 2014, **136**, 1643–1649.
117 G. Singh, A. Singh, G. Sharma, S. C. Sahoo and A. Kaur, *J. Mol. Struct.*, 2021, **1229**, 129618.
118 A. Varghese and K. Akshaya, *Rev. Fluoresc.*, 2018, **2017**, 99–121.
119 J. E. Kwon and S. Y. Park, *Adv. Mater.*, 2011, **23**, 3615–3642.
120 P. Zhou and K. Han, *Acc. Chem. Res.*, 2018, **51**, 1681–1690.
121 H. Sun, S.-S. Sun, F.-F. Han, Y. Zhao, B.-X. Miao, J. Nie, R. Zhang and Z.-H. Ni, *J. Chem. Eng.*, 2021, **405**, 127000.
122 S. Ghosh, D. Singharoy, S. Konar, J. P. Naskar and S. C. Bhattacharya, *J. Coord. Chem.*, 2021, **74**, 1272–1283.
123 M. N. El-Nahass, *J. Mol. Struct.*, 2024, **1318**, 139273.
124 G. T. Tigineh and L.-K. Liu, *J. Photochem. Photobiol., A*, 2017, **338**, 161–170.
125 N. Sharma and N. Sandhu, *J. Photochem. Photobiol., A*, 2024, **457**, 115903.
126 R. D. Cowan and G. H. Dieke, *Rev. Mod. Phys.*, 1948, **20**, 418.
127 H.-W. Zheng, D.-D. Yang, Y.-S. Shi, T. Xiao, H.-W. Tan and X.-J. Zheng, *Inorg. Chem.*, 2023, **62**, 6323–6331.
128 H.-W. Zheng, M. Wu, S.-J. Liu, Y.-H. Fang, X.-B. Deng and X.-J. Zheng, *Cryst. Growth Des.*, 2025, **25**, 1842–1850.
129 M. S. Abdelaty, *Polym. Bull.*, 2023, **80**, 5759–5783.
130 M. Gaeta, I. P. Oliveri, G. Munzi, F. Lo Presti and S. Di Bella, *Inorg. Chem.*, 2024, **63**, 3850–3858.
131 A. Attinà and I. P. Oliveri, *Sens. Actuators, B*, 2024, **419**, 136414.
132 X. Wang, Z. Z. Li, S. F. Li, H. Li, J. Chen, Y. Wu and H. Fu, *Adv. Opt. Mater.*, 2017, **5**, 1700027.
133 P. Gayathri, M. Pannipara, A. G. Al-Sehemi and S. P. Anthony, *CrystEngComm*, 2021, **23**, 3771–3789.
134 B. Tang, H. Zhang, K. Ye, H. Zhang and Y. Wang, *Chem. Commun.*, 2016, **52**, 13128–13131.
135 F. Liu, J. Tu, X. Wang, J. Wang, Y. Gong, M. Han, X. Dang, Q. Liao, Q. Peng and Q. Li, *Chem. Commun.*, 2018, **54**, 5598–5601.
136 Y. Qian, S. Li, G. Zhang, Q. Wang, S. Wang, H. Xu, C. Li, Y. Li and G. Yang, *J. Phys. Chem. B*, 2007, **111**, 5861–5868.
137 V. S. Padalkar and S. Seki, *Chem. Soc. Rev.*, 2016, **45**, 169–202.
138 C. Azarias, Š. Budzák, A. D. Laurent, G. Ulrich and D. Jacquemin, *Chem. Sci.*, 2016, **7**, 3763–3774.
139 C.-L. Chen, Y.-T. Chen, A. P. Demchenko and P.-T. Chou, *Nat. Rev. Chem.*, 2018, **2**, 131–143.
140 J. Goodman and L. Brus, *J. Appl. Chem. Sci.*, 1978, **100**, 7472–7474.
141 S. Dogra, *J. Photochem. Photobiol., A*, 2005, **172**, 196–206.
142 K.-i Sakai, S. Tsuchiya, T. Kikuchi and T. Akutagawa, *J. Mater. Chem. C*, 2016, **4**, 2011–2016.
143 K.-C. Tang, M.-J. Chang, T.-Y. Lin, H.-A. Pan, T.-C. Fang, K.-Y. Chen, W.-Y. Hung, Y.-H. Hsu and P.-T. Chou, *J. Appl. Chem. Sci.*, 2011, **133**, 17738–17745.
144 H. Shono, T. Ohkawa, H. Tomoda, T. Mutai and K. Araki, *ACS Appl. Mater. Interfaces*, 2011, **3**, 654–657.
145 L. Chen, S.-Y. Yin, M. Pan, K. Wu, H.-P. Wang, Y.-N. Fan and C.-Y. Su, *J. Mater. Chem. C*, 2016, **4**, 6962–6966.
146 S.-Y. Yin, S.-S. Sun, M. Pan, L. Chen, Z. Wang, Y.-J. Hou, Y.-N. Fan, H.-P. Wang and C.-Y. Su, *J. Photochem. Photobiol., A*, 2018, **355**, 377–381.
147 Y.-H. Luo, J.-W. Wang, W. Wang, X.-T. He, D.-L. Hong, C. Chen, T. Xu, Q. Shao and B.-W. Sun, *ACS Appl. Mater. Interfaces*, 2018, **10**, 16666–16673.
148 Y.-H. Luo, C. Chen, G.-W. Lu, D.-L. Hong, X.-T. He, C. Wang, J.-Y. Wang and B.-W. Sun, *J. Phys. Chem. Lett.*, 2018, **9**, 7052–7058.
149 J.-Y. Wang, C. Chen, C. He, Z.-Y. Zheng, C. Wang, D.-L. Hong, X.-T. He, Y.-H. Luo and B.-W. Sun, *J. Mater. Chem. C*, 2019, **7**, 3965–3972.
150 Z. Zhang, J. Huang, Y. Fang, M. Zhang, K. Liu and B. Dong, *Adv. Mater.*, 2017, **29**, 1606688.
151 S. K. Thiyagarajan, R. Suresh, V. Ramanan and P. Ramamurthy, *Chem. Sci.*, 2018, **9**, 910–921.
152 H. Konoshima, S. Nagao, I. Kiyota, K. Amimoto, N. Yamamoto, M. Sekine, M. Nakata, K. Furukawa and H. Sekiya, *Phys. Chem. Chem. Phys.*, 2012, **14**, 16448–16457.
153 P. B. Bisht, H. Petek, K. Yoshihara and U. Nagashima, *J. Chem. Phys.*, 1995, **103**, 5290–5307.
154 F. Lahmani and A. Zehnacker-Rentien, *J. Phys. Chem. A*, 1997, **101**, 6141–6147.
155 S. Ameer-Beg, S. M. Ormson, X. Poteau, R. G. Brown, P. Foggi, L. Bussotti and F. V. Neuwahl, *J. Phys. Chem. A*, 2004, **108**, 6938–6943.
156 M. Itoh, K. Tokumura, Y. Tanimoto, Y. Okada, H. Takeuchi, K. Obi and I. Tanaka, *J. Appl. Chem. Sci.*, 1982, **104**, 4146–4150.
157 P. Purkayastha and N. Chattopadhyay, *Phys. Chem. Chem. Phys.*, 2000, **2**, 203–210.

158 H. Xiao, K. Chen, D. Cui, N. Jiang, G. Yin, J. Wang and R. Wang, *New J. Chem.*, 2014, **38**, 2386–2393.
159 Y. Houari, A. Charaf-Eddin, A. D. Laurent, J. Massue, R. Ziessel, G. Ulrich and D. Jacquemin, *Phys. Chem. Chem. Phys.*, 2014, **16**, 1319–1321.
160 F. S. Rodembusch, F. P. Leusin, L. F. da Costa Medina, A. Brandelli and V. Stefani, *Photochem. Photobiol. Sci.*, 2005, **4**, 254–259.
161 P.-T. Chou, Y.-C. Chen, W.-S. Yu, Y.-H. Chou, C.-Y. Wei and Y.-M. Cheng, *J. Phys. Chem. A*, 2001, **105**, 1731–1740.
162 V. S. Padalkar, A. Tathe, V. D. Gupta, V. S. Patil, K. Phatangare and N. Sekar, *J. Fluoresc.*, 2012, **22**, 311–322.
163 A. Ohshima, A. Momotake, R. Nagahata and T. Arai, *J. Phys. Chem. A*, 2005, **109**, 9731–9736.
164 S. Barman, S. K. Mukhopadhyay, M. Gangopadhyay, S. Biswas, S. Dey and N. P. Singh, *J. Mater. Chem. B*, 2015, **3**, 3490–3497.
165 N. A. Shekhovtsov and M. B. Bushuev, *J. Mol. Liq.*, 2022, **361**, 119611.
166 J. Huang, N. Sun, J. Yang, R. Tang, Q. Li, D. Ma and Z. Li, *Adv. Funct. Mater.*, 2014, **24**, 7645–7654.
167 H. Wu, X. C. Fan, H. Wang, F. Huang, X. Xiong, Y. Z. Shi, K. Wang, J. Yu and X. H. Zhang, *Aggregate*, 2023, **4**, e243.
168 G. Yang, Y. Ran, Y. Wu, M. Chen, Z. Bin and J. You, *Aggregate*, 2022, **3**, e127.
169 Y. Li, R. Zhang, Q. Wan, R. Hu, Y. Ma, Z. Wang, J. Hou, W. Zhang and B. Z. Tang, *Adv. Sci.*, 2021, **8**, 2102561.
170 J. Zhao, S. Ji, Y. Chen, H. Guo and P. Yang, *Phys. Chem. Chem. Phys.*, 2012, **14**, 8803–8817.
171 Y. Ooyama, Y. Kagawa, H. Fukuoka, G. Ito and Y. Harima, *Eur. J. Org. Chem.*, 2009, 5321–5326.
172 Y. Ooyama and Y. Harima, *J. Mater. Chem.*, 2011, **21**, 8372–8380.
173 S. Lü, C. Gao, X. Xu, X. Bai, H. Duan, N. Gao, C. Feng, Y. Xiong and M. Liu, *ACS Appl. Mater. Interfaces*, 2015, **7**, 13029–13037.
174 N. Artzi, T. Shazly, A. B. Baker, A. Bon and E. R. Edelman, *Adv. Mater.*, 2009, **21**, 3399.
175 J. Huang, Y. Deng, J. Ren, G. Chen, G. Wang, F. Wang and X. Wu, *Carbohydr. Polym.*, 2018, **186**, 54–63.
176 Y.-H. Ma, J. Yang, B. Li, Y.-W. Jiang, X. Lu and Z. Chen, *Polym. Chem.*, 2016, **7**, 2037–2044.
177 J. Tang, M. U. Javaid, C. Pan, G. Yu, R. M. Berry and K. C. Tam, *Carbohydr. Polym.*, 2020, **229**, 115486.
178 C. Xu, W. Zhan, X. Tang, F. Mo, L. Fu and B. Lin, *Polym. Test.*, 2018, **66**, 155–163.
179 Q. Li, C. Liu, J. Wen, Y. Wu, Y. Shan and J. Liao, *Chin. Chem. Lett.*, 2017, **28**, 1857–1874.
180 M. Vahedi, J. Barzin, F. Shokrolahi and P. Shokrollahi, *Macromol. Mater. Eng.*, 2018, **303**, 1800200.
181 S. Zhang, D. Huang, H. Lin, Y. Xiao and X. Zhang, *Biomacromolecules*, 2020, **21**, 2400–2408.
182 M. M. Perera and N. Ayres, *Polym. Chem.*, 2020, **11**, 1410–1423.
183 S. K. Panja, *Spectrochim. Acta, Part A*, 2020, **229**, 117860.
184 G. Kaştaş, Ç. A. Kaştaş and A. Tabak, *Spectrochim. Acta, Part A*, 2019, **222**, 117198.
185 J. Shu, T. Ni, X. Liu, B. Xu, L. Liu, W. Chu, K. Zhang and W. Jiang, *Dyes Pigm.*, 2021, **195**, 109708.
186 G.-H. Ning, Z. Chen, Q. Gao, W. Tang, Z. Chen, C. Liu, B. Tian, X. Li and K. P. Loh, *J. Appl. Chem. Sci.*, 2017, **139**, 8897–8904.
187 G. Huang, X. Du, H. Bo and B. S. Li, *Mater. Chem. Front.*, 2024, **8**, 104–132.
188 Y. Chen, Y. R. Lee, W. Wang, Y. Fang, S. Lu, J. Han, X. Chen, M. H. Kim and J. Yoon, *Angew. Chem., Int. Ed.*, 2023, **62**, e202301765.
189 X.-M. Cai, Y. Lin, Z. Tang, X. Zhang, T. Mu, S. Huang, Z. Zhao and B. Z. Tang, *J. Chem. Eng.*, 2023, **451**, 138627.
190 Y. Liu, X. Liu, Y. Tian, R. Ran, C. Du, Y. Wang, N. Ma, R. Li, X. Chai and X. Dong, *Mater. Today Chem.*, 2024, **40**, 102241.
191 K. Chaihan, N. Semakul, V. Promarak, T.-T. Bui, N. Kungwan and F. Goubard, *J. Photochem. Photobiol., A*, 2022, **431**, 114047.
192 X. Hu, H. Chen, L. Zhao, M. Miao and Y. Zheng, *Chem. Mater.*, 2019, **31**, 10256–10262.
193 Y. Wang, Y. Z. Cheng, K. M. Wu, D. H. Yang, X. F. Liu, X. Ding and B. H. Han, *Angew. Chem., Int. Ed.*, 2023, **135**, e202310794.
194 G. Yakalı, *Phys. Chem. Chem. Phys.*, 2021, **23**, 11388–11399.
195 J. C. Del Valle and J. Catalán, *Phys. Chem. Chem. Phys.*, 2019, **21**, 10061–10069.
196 A. P. Demchenko, V. I. Tomin and P.-T. Chou, *Chem. Rev.*, 2017, **117**, 13353–13381.
197 L. Shi, C. Yan, Z. Guo, W. Chi, J. Wei, W. Liu, X. Liu, H. Tian and W.-H. Zhu, *Nat. Commun.*, 2020, **11**, 793.
198 Y. Zhou, G. Baryshnikov, X. Li, M. Zhu, H. Ågren and L. Zhu, *Chem. Mater.*, 2018, **30**, 8008–8016.
199 Y. H. Wu, H. Xiao, B. Chen, R. G. Weiss, Y. Z. Chen, C. H. Tung and L. Z. Wu, *Angew. Chem., Int. Ed.*, 2020, **59**, 10173–10178.
200 S. M. Borisov, R. Pommer, J. Svec, S. Peters, V. Novakova and I. Klimant, *J. Mater. Chem. C*, 2018, **6**, 8999–9009.
201 Z. Yu, Q. Li, X. He, X. Wang, Y. Wen, L. Zeng, W. Yu, P. Hu and H. Chen, *Eur. Polym. J.*, 2023, **197**, 112330.
202 D. Shen, W. Jin, Q. Zhao, M. Wang, B. Zhang, H. Feng, W. Wan, Y. Bai, H. Lyu and J. Sun, *Anal. Chem.*, 2022, **94**, 14143–14150.
203 S. K. Kushvaha, B. Shankar, N. S. M. Gorantla and K. C. Mondal, *ChemistrySelect*, 2019, **4**, 3334–3339.
204 Q.-H. Zhu, G.-H. Zhang, L. Zhang, S.-L. Wang, J. Fu, Y.-H. Wang, L. Ma, L. He and G.-H. Tao, *J. Appl. Chem. Sci.*, 2023, **145**, 6177–6183.
205 A. Steinegger and S. M. Borisov, *ACS Omega*, 2020, **5**, 7729–7737.
206 J. Liu, X. Zhang, X. Chen, L. Qu, L. Zhang, W. Li and A. Zhang, *Polym. Chem.*, 2018, **9**, 378–387.
207 Z. Q. Lei, P. Xie, M. Z. Rong and M. Q. Zhang, *J. Mater. Chem. A*, 2015, **3**, 19662–19668.
208 X. Gong, Z. Cheng, S. Gao, D. Zhang, Y. Ma, J. Wang, C. Wang and F. Chu, *Carbohydr. Polym.*, 2020, **250**, 116846.
209 X. H. Ding, L. Z. Wang, Y. Z. Chang, C. X. Wei, J. Y. Lin, M. H. Ding and W. Huang, *Aggregate*, 2024, **5**, e500.
210 X. Ding, G. Li, C. Xiao and X. Chen, *Macromol. Chem. Phys.*, 2019, **220**, 1800484.
211 A. Jiménez-Sánchez, N. Farfán and R. Santillan, *J. Phys. Chem. C*, 2015, **119**, 13814–13826.